ISSN 0915-6364

NATIONAL INSTITUTE FOR FUSION SCIENCE

Collision Processes of Li^{3+} with Atomic Hydrogen: Cross Section Database

I. Murakami , J. Yan , H. Sato , M. Kimura , R. K. Janev , T. Kato

(Received - May 27, 2004)

NIFS-DATA-86 Aug. 2004

TOKI, JAPAN

Collision Processes of Li^{3+} with Atomic Hydrogen: Cross Section Database

I.Murakami[1], J. Yan[2], H. Sato[3], M. Kimura[4], R. K. Janev[1,5], T. Kato[1]

1) National Institute for Fusion Science, Oroshi, Toki, Gifu,509-5292, Japan
2) Institute of Applied Physics and Computational Mathematics, Beijing 100088, China
3) Ochanomizu Woman University, Tokyo, 112-8611, Japan
4) Yamaguchi University, Ube, Yamaguchi, 755-8611, Japan
5) Macedonian Academy of Sciences and Arts, 1000 Skopje, Macedonia

Abstract

Using the available experimental and theoretical data, as well as established cross section scaling relationships, a cross section database for excitation, ionization and charge exchange in collisions of Li^{3+} ion with ground state and excited hydrogen atoms has been generated. The critically assessed cross sections are represented by analytic fit functions that have correct asymptotic behavior both at low and high collision energies.

The derived cross sections are also presented in graphical form.

PACS: 34.50Fa, 52.20Hv

Keywords: Hydrogen atom, Lithium ion, Excitation, Ionization, Charge exchange, Cross sections, Collision processes

1. Introduction

Collision processes of Li^{3+} ions with atomic hydrogen are of interest in magnetic fusion energy research in the context of TESPEL based CXRS plasma diagnostic and transport studies [1,2] and proposed liquid lithium plasma facing divertor concepts [3,4].
Processes of interest include:

$$Li^{3+} + H(n_0 \geq 1) \rightarrow Li^{3+} + H(n > n_0), \quad (1)$$
$$Li^{3+} + H(n_0 \geq 1) \rightarrow Li^{3+} + H^+ + e, \quad (2)$$
$$Li^{3+} + H(n_0 \geq 1) \rightarrow Li^{2+}(n'\ell') + H^+, \quad (3)$$

where $n(n_0)$ and ℓ are the usual quantum numbers of electronic states.
In this report we present a complete set of cross sections for the processes (1)-(3). As basis for this cross section set we have used the available experimental and theoretical data from the literature, critically assessed for their accuracy, and appropriate, well-established cross section scaling relationships. Most of the available data are pertinent to the initial $n_0\ell_0$=1s state of hydrogen atom. The data sources for each of processes (1)-(3), and the method (procedure) of evaluation or derivation of the cross section for each particular reaction, will be discussed in detail in the sections that follow. For each cross section we shall provide also information about its estimated accuracy.
The evaluated (or derived) cross sections of individual reactions within processes (1)-(3) for the lower initial levels n_0 are presented by analytic fit functions that have correct physical behavior at both low and high collision energies. For the cross sections with high initial n_0, appropriate scaling relations are used.

2. Excitation

2.1. Excitation from the ground state ($n_0\ell_0$ = 1s)

Cross section measurements for Li^{3+} induced $1s \rightarrow n(\geq 2)$ transitions do not exist in the literature. There are two sets of cross section calculations by the

adiabatic superpromotion model for $1s \rightarrow n=2$ [5] and by the atomic orbital close coupling (AOCC) model (with 24 AOs) for $1s \rightarrow n = 2,3$ [6]. There are also cross section calculations for $1s \rightarrow n (\leq 4)$ induced by A^{q+} fully stripped ions with q=2,4,6,8,14,and 26 performed by two-center atomic orbital close-coupling (2C-AOCC) and classical trajectory Monte Carlo (CTMC) method [7,8] in the intermediate to high energy range (~ 10keV/amu—800keV/amu), and "hidden-crossings" superpromotion method [9,10] (for q=2,4 only) at low collision energies (≤25 keV/amu). (More detailed information on this and other work is given in [11].)

The results of these extensive calculations show that for a given $1s \rightarrow n$ transition the excitation cross section $\sigma_{exc}^{(q)}(n)$ scales with q, for $q \geq 2$, as [11]

$$\sigma_n^{(q)} \backsim q\,\chi(q)\,\sigma_n^{(2)}(E/q), \quad E/q \geq 10 \text{ keV/amu} \tag{4a}$$

$$\sigma_n^{(q)} \backsim q\,\chi(q)\,\sigma_n^{(2)}(E), \quad E/q \leq 10 \text{ keV/amu} \tag{4b}$$

where $\chi(q)=2^{0.5238(1-\sqrt{2/q})}$.

2.1.1. Transitions to $n = 2,3,4$ levels

The cross sections for $1s \rightarrow n=2,3,4$ transitions in H by Li^{3+} impact have been determined by using the data from [5] and [6] (for $n=2,3$) and scaling the corresponding recommended cross sections for He^{2+} and Be^{4+} impact [11] according to the relations (4) and, then taking the average of obtained scaled cross sections. The obtained excitation cross sections are fitted by the analytic expression ($n=2,3,4$)

$$\sigma_n^{(q)}(n) = a_1\left[\frac{\exp(-a_2/E)\ell n(1+a_3E)}{E} + \frac{a_4\exp(-a_5E)}{E^{a_6}} + \frac{a_7\exp(-a_8/E)}{1+a_9E^{a_{10}}}\right] \quad (\times 10^{-16} cm^2) \tag{5}$$

where E is expressed in keV/amu units, and the values of fitting parameters a_i are given in Table 1. The rms deviation of the fits is smaller than 1% for all n. Comparison between the fitting line and the theoretical results of Ref.

[5,6] is also displayed in Figure 1 for 1s-n=2 excitation. We note that $\sigma_{exc}(n=2)$ given by Esq. (5) agrees well with the results of superpromotion model [5] for E ≤ 25 keV/amu. The accuracy of the cross sections given by Eq. (5) and Table 1 should be close to the accuracy of corresponding cross sections for He^{2+} and Be^{4+} impact, from which they have been derived. For E ≤ 20 keV/amu, their uncertainty (defined as combined experimental and/or theoretical error) is 30-80%, for 20 ≤ E(keV/amu) ≤ 200 it is 20-30%, and for E ≥ 200 keV/amu it is expected to be 15-20%, or better.

2.1.2. Transitions to n = 5,6 levels

The cross sections for the transitions 1s→n=5,6 have been determined by using the corresponding He^{2+} impact data from [11] and the scaling relations (4). These cross sections have somewhat simpler structure and can be fitted by the expression (n=5,6)

$$\sigma_{exc}(n) = b_1\left[\frac{\exp(-b_2/E)\ell n(1+b_3E)}{E} + \frac{b_4\exp(-b_5E)}{E^{b_6}+b_7E^{b_8}}\right] \quad (\times 10^{-16} cm^2) \qquad (6)$$

where E is in keV/amu units. The values of fitting parameters b_i in Eq. (6) are given in Table 2. The rms deviation of the fits is smaller than 1%.
The expected uncertainty of the cross sections given by Eq. (6) and Table 2 is 40-100% for E < 5keV/amu, 30-40% for 5 ≤E (keV/amu) ≤ 20, 30-40% for 20 ≤E (keV/amu) ≤ 200, and better than 20% for E > 200 keV/amu.

2.1.3. Transitions to n ≥ 7 levels

The cross sections for 1s→n ≥ 7 excitation transitions can be obtained by using the well-known scaling relation (see, e.g., [11])

$$\sigma_{exc}(n \geq 7) = \left(\frac{6}{n}\right)^3 \sigma_{exc}(1s \rightarrow n=6), \qquad (7)$$

which should be accurate for E ≥ 20 keV/amu. Given the large uncertainty (>30%) of σ_{exc}(1s→ n =6) cross section for E ≤ 20 keV/amu, the scaling

formula (7) can be safely used also for E $\lesssim$ 20keV/amu.

2.2. Excitation from $n_0 \geq 2$ levels

Specific cross section measurements or calculations for transitions from the $n_0 \geq 2$ levels of H by Li^{3+} impact do not exist in the literature. Calculations exist only for the transitions from $n_0\ell_0 = 2s$ to higher $n\ell$ states, performed by the superpromotion model in the low energy region [12]. The contribution from the $n_0\ell_0 = 2p$ state to the total excitation cross section from the $n_0 = 2$ level to any higher level is expected to be significant. Total excitation cross section from the levels $n_0 = 2$ and $n_0 = 3$, however, do exist for He^{2+} [9] and Be^{4+} [10] impact. In determining the Li^{3+} impact excitation cross sections from $n_0 = 2,3$ we shall use these data.

2.2.1. Excitation from $n_0 = 2$ level

a) Transitions to $n = 3,4,5$ levels

The cross sections for transitions $n_0 = 2 \rightarrow n = 3,4,5$ have been determined by scaling the corresponding cross section data for He^{2+} and Be^{4+} impact from [11] according to Eqs. (4), and taking their average. The obtained cross sections have been then fitted to the expression (n=3,4,5)

$$\sigma_{exc}(2 \rightarrow n) = c_1\left[\frac{\exp(-c_2/E)\ell n(1+c_3E)}{E} + \frac{c_4\exp(-c_5E)}{E^{c_6}}\right] \quad \left(\times 10^{-16} cm^2\right) \qquad (8)$$

with collision energy E expressed in keV/amu. The values of fitting parameters c_i are given in Table 3, and the rms deviation of the fit is well below 1%. The uncertainty of the data is expected to be 40-80% for E $\lesssim$ 5keV/amu, 30-40% for 5 $\leq$ E(keV/amu) $\leq$ 20, 20-30% for 20 $\leq$ E(keV/amu) $\leq$200 and 15-20% for E $\geq$ 200 keV/amu.

b) Transitions to $n \geq 6$ levels

The cross sections for $n_0 = 2 \rightarrow n = 6$-10 transitions have been determined by scaling the corresponding cross sections for He^{2+} (or proton) impact from Ref.

[11] according to Eq. (4a). The obtained cross sections can be expressed in the form

$$\sigma_{exc}(2 \rightarrow n = 6-10) = c_{2-n}\sigma_{exc}(2 \rightarrow 5) \qquad (9)$$

where coefficients c_{2-n} have the values given in Table 4.
For the transitions $n_0 = 2 \rightarrow n \geq 11$, one can use the n^{-3} -scaling,

$$\sigma_{exc}(2 \rightarrow n) = \left(\frac{10}{n}\right)^3 \sigma_{exc}(2 \rightarrow 10) \quad , \quad n > 10 \qquad (10)$$

The uncertainty of the cross sections given by Eqs. (9) and (10) should be by 5-10% higher than that for $\sigma_{exc}(2 \rightarrow 5)$.

2.2.2. Transitions from $n_0 = 3$

a) Transitions to $n = 4,5,6$ levels

For the $n_0 = 3 \rightarrow n = 4,5,6$ transitions in H, induced by Li^{3+} impact, the cross sections have been determined as an average of the corresponding He^{2+} and Be^{4+} impact cross sections of Ref. [11], scaled according Eq. (4a). So derived cross sections were then fitted to an expression having the same form as Eq. (8). The values of fitting parameters c_i are given in Table 5. The uncertainty of derived cross sections is 40-80% for E ≤ 5keV/amu, 30-40% for 5 ≤ E(keV/amu) ≤ 100, and 20-30% for E ≥ 100keV/amu.

b) Transitions to $n \geq 7$ levels

The cross sections for $n_0 = 3 \rightarrow n = 7$-10 transitions have been determined by scaling the corresponding He^{2+} impact cross sections of Ref. [11] according to Eq. (4a). The obtained cross sections can be expressed in the form

$$\sigma_{exc}(3 \rightarrow n = 7-10) = c_{3-n}\sigma_{exc}(3 \rightarrow 6) \qquad (11)$$

where the coefficients c_{3-n} for n = 7,8,9,10 have the values given in Table 6. For the transitions to $n \geq 11$ levels, the cross sections can be evaluated by using the n^{-3} -scaling

$$\sigma_{exc}(3 \to n) = \left(\frac{10}{n}\right)^3 \sigma_{exc}(3 \to 10), \quad n > 10 \tag{12}$$

The uncertainty of the cross sections given by Eqs. (11) and (12) is expected to be by 5-10% higher than that for $\sigma_{exc}(3 \to 6)$.

2.2.3. Transitions from $n_0 \geq 4$

In absence of any systematic cross section data for transitions from $n_0 \geq 4$ levels, the q-scaled proton-impact semi-empirical formula of Lodge et al. [13] can be used. In order to account for the small deviations of the q-scaling at large energies and for high ionic charge q, a correction factor $\xi(q)$ has been introduced in Ref. [11]

$$\xi(q) = 2^{0.322\left(1-\sqrt{2/q}\right)} \tag{13}$$

which for q = 3 is $\xi(3) \cong 1.042$. The q - scaled Lodge et al. formula [11] for q=3 and the $n_0 \to n$ transition can be written as

$$\sigma_{exc}(n_0 \to n) = 2.769 \frac{n_0^4}{\varepsilon}[ADL + FGH] \qquad \left(\times 10^{-16} cm^2\right) \tag{14}$$

where

$$\varepsilon = \frac{E(keV/amu)}{75}, \quad s = n - n_0, \quad D = \exp\left[-\frac{1}{n_0 n \varepsilon^2}\right],$$

$$A = \frac{8}{3s}\left(\frac{n}{s n_0}\right)^3 \left(0.184 - \frac{0.04}{s^{2/3}}\right)\left(1 - \frac{0.2s}{n_0 n}\right)^{1+2s}, \quad G = \frac{1}{2}\left(\frac{\varepsilon n_0^2}{n - 1/n}\right)^3,$$

$$L = \ell n\left(\frac{1+0.53\varepsilon^2 n_0(n-2/n)}{1+0.4\varepsilon}\right),\quad F = \left(1-\frac{0.3sD}{n_0 n}\right)^{1+2s},$$

$$H = \left|c_2\left(z^{(-)},y\right)-c_2\left(z^{(+)},y\right)\right|,\quad c_2(z,y) = \frac{z^2\ell n(1+2z/3)}{2y+3z/2},$$

$$z^{(\pm)} = \frac{2}{\varepsilon n_0^2\left[\left(2-\frac{n_0^2}{n^2}\right)^{1/2}\pm 1\right]},\quad y = \frac{1}{1-D\ell n(18s)/4s}.$$

The accuracy of the cross sections given by Eq. (14) is expected to be by 5-10% worse than for the $\sigma_{exc}(2\to 5)$ or $\sigma_{exc}(3\to 6)$ cross sections.

3. Ionization

3.1. Ionization from the ground state ($n_0\ell_0$ = 1s)

The ionization of H(1s) by Li^{3+} impact has been subject to extensive both experimental and theoretical studies. The experimental cross section measurements exist in the energy range 50 – 500 keV/amu [14,15] and have accuracy on the level 10%. Theoretical cross section calculations have been performed by using the adiabatic superpromotion model [5], atomic-orbital close-coupling (AOCC) method [6,16], molecular-orbital close-coupling (MOCC) method [17], classical trajectory Monte Carlo (CTMC) method [18] and continuum distorted wave (CDW) method [19]. These results are plotted in figure 2, as well as the fitting line using the formula described below. The theoretical calculations cover the energy range from ~1 keV/amu to ~ 650 keV/amu, and agree with each other within 10-20% in the overlapping regions of their validity. While the MOCC method is valid at energies below ~ 25 keV/amu, the AOCC method (with a large expansion basis) should be valid down to ~1-5 keV/amu. The validity of CTMC methods is restricted to the range ~30-200 keV/amu, while CDW is a typical high-energy method valid for E ≥ 150-200 keV/amu. For E > 200-300 keV/amu, the Bethe-Born approximation (BBA) should also be valid. The BBA gives the ionization cross section for H(1s) in closed form for any fully stripped ion [20] (q-scaled

cross section). It should be noted that the low-energy ionization cross section for H(1s) by fully stripped ion impact allows also a q-scaled representation [21]. The Li^{3+} +H(1s) ionization cross section recommended for use is based on the very extensive AOCC calculations [16], experimental data [14,15], and CDW and q-scaled BBA cross sections. The AOCC cross section for E ≤ 20 keV/amu is consistent with the cross section derived from the adiabatic superpromotion data [5] and q-scaling formula [21]. So determined "recommended" ionization cross section for H(1s) by Li^{3+} impact was fitted to the analytic expression ($n_0 = 1$)

$$\sigma_{ion}(n_0) = a_1\left[\frac{\exp(-a_2/E)\ell n(1+a_3E)}{E} + \frac{a_4\exp(-a_5E)}{E^{a_6}+a_7E^{a_8}}\right] \quad \left(\times 10^{-16} cm^2\right) \qquad (15)$$

where the collision energy is in keV/amu units and the values of fitting parameters are given in Table 7. The rms deviation of the fit is about 5%, most of it generated in the range 7-30 keV/amu where the AOCC cross section data are about 10-20% below the fit. By choosing a more complicated fit expression for $\sigma_{ion}(1s)$ (such as given by Eq. (5), for instance), the rms could be reduced to a much lower level. However, for the sake of uniformity with fitting expressions for $\sigma_{ion}(n0)$, for n_0=2,3, (see next subsection), we have kept the fit of $\sigma_{ion}(1s)$ in the form of Eq. (15). The estimated uncertainty of $\sigma_{ion}(1s)$ is 15-20% for E ≤ 50 keV/amu and 10-15% for E ≥ 50 keV/amu.

3.2. Ionization from $n_0 \geq 2$ levels

3.2.1. Ionization from $n_0 = 2$ and $n_0 = 3$

There are no cross section data for Li^{3+} impact ionization of $H(n_0)$ for the n_0 = 2, 3 levels. A single cross section calculation exists for the metastable 2s state, performed within the adiabatic superpromotion model [12].

The cross section $\sigma_{ion}(n_0 = 2)$ was determined by scaling the corresponding cross section for He^{2+} impact from Ref. [11] according to scaling relation [22,23]

$$\frac{\sigma_{ion}(q,n_0)}{qn_0^4} = f\left(n_0^2 E/q\right), \tag{16}$$

The cross section $\sigma_{ion}(n_0 = 3)$ at high energies was determined from the scaled BBA formula (see [11]), and at low energies (below ~ 20keV/amu) by using the ratio

$$\frac{\sigma_{ion}\left(Li^{3+};n_0 = 3\right)}{\sigma_{ion}\left(Li^{3+};n_0 = 2\right)} = \frac{\sigma_{ion}\left(He^{2+};n_0 = 3\right)}{\sigma_{ion}\left(He^{2+};n_0 = 2\right)} \tag{17}$$

in which $\sigma_{ion}\left(He^{2+};n_0 = 2,3\right)$ were taken from Ref. [11].
The cross sections $\sigma_{ion}(n_0 = 2,3)$ derived in this way have been fitted to an expression of the form given by Eq. (15). The corresponding fitting coefficients a_i are given in Table 7. The uncertainty of $\sigma_{ion}(n_0 = 2,3)$ cross sections is estimated to be 30-40% for E≤10 keV/amu, 20-30% for 10 ≤ E(keV/amu) ≤ 100, and ~20% for E ≥ 100 keV/amu.

3.2.2. Ionization from $n_0 \geq 4$ levels

The cross section $\sigma_{ion}(n_0 \geq 4)$ can be derived by using the scaling relation

$$\sigma_{ion}\left(n_0;E_{n_0}\right) = \left(\frac{n_0}{3}\right)^4 \sigma_{ion}\left(n_0 = 3;E\right), \quad E_{n_0} = \left(\frac{3}{n_0}\right)^2 E \tag{18}$$

where $\sigma_{ion}(n_0 = 3;E)$ is the ionization cross section for n_0 = 3 level given in the preceding sub-section. The scaling relation (18) should be fairly accurate (~10% uncertainty) for E n_0 ≥ 100 keV/amu, but it becomes less accurate at lower energies.

4. Electron Capture

4.1. Electron capture from H(1s)

Electron capture in Li^{3+} + H(1s) collisions has been subject to many both

theoretical and experimental studies. The motivation for this is the fact that at low and intermediate collision energies the electron capture process populates dominantly the excited states of $Li^{2+}(n\ell)$ ion, the radiation from which can be used for diagnostic purposes (see, e.g., [1,2]). As a result of these studies, both the total and state-selective (for a given $n\ell$), cross sections for this process are known to a high accuracy in the energy range from ~100 eV/amu to 10 MeV/amu.

4.1.1. Total cross section

There have been two experimental measurements of the total cross section of Li^{3+} + H(1s) charge exchange reaction covering the energy ranges 15-250 keV/amu[14] and ~ 1-6 keV/amu [24]. Theoretical calculations are numerous; they employ different types of methods with varying accuracy and taken together, cover the energy range from 80 eV/amu to 10 MeV/amu. The most accurate of these calculations agree with each other, as well as with the experimental data (except for the lower measured energies of Ref. [24]).
The total charge exchange (CX) cross section is sum over the electron capture cross sections to specific (n,ℓ) final states, $\sigma_{CX}^{(n,\ell)}$, of product ion $Li^{2+}(n\ell)$,

$$\sigma_{CX}^{tot} = \sum_{n,\ell} \sigma_{CX}^{(n,\ell)} = \sum_{n} \sigma_{CX}^{(n)} \tag{19}$$

where

$$\sigma_{CX}^{(n)} = \sum_{\ell} \sigma_{CX}^{(n,\ell)} \tag{20}$$

is the electron capture cross section to all ℓ-sub-states within a given n-shell. Since in most applications (e.g. CX recombination spectroscopy, CXRS) $\sigma_{CX}^{(n,\ell)}$ are of main interest, we present in the next sub-section the best available theoretical information for $\sigma_{CX}^{(n,\ell)}$. The total cross section σ_{CX}^{tot} is then obtained from Eq. (19).

4.1.2. $\sigma_{CX}^{(n,\ell)}$ and $\sigma_{CX}^{(n)}$ partial cross sections

While experimental measurements of state-selective electron capture cross sections $\sigma_{CX}^{(n,\ell)}$ in reaction (3) have not yet been reported, there have been many theoretical calculations of these cross sections, several of them having high accuracy (≤10% uncertainty) in the energy region of their applicability.

In the low energy region (E ≤ 20keV/amu), accurate calculations of $\sigma_{CX}^{(n,\ell)}$ have been performed by the advanced adiabatic (superpromotion) method [5] and by the MO-CC method employing large number of MOs [25,26]. The calculations in Ref. [26] go down to energies of ~80 eV/amu. In the intermediate-to-high energy region (E≈15-200 keV/amu), there exist a number of large-base AO-CC calculations of $\sigma_{CX}^{(n,\ell)}$ [6,27,27a,28], some of them employing also a large number of pseudo-states [27,27a,28]. In this energy range (but above 37.5 keV/amu) there exist also extensive CTMC calculations [29], some of them being performed (for the n=6 states) in the course of the present work. For the capture to 2s state, a cross section calculation has been performed in Ref. [30] by a second-order type method.

In the high-energy region (E ≥ 100 keV/amu), accurate $\sigma_{CX}^{(n,\ell)}$ cross sections for the reaction (3) have been performed within the second-order continuum distorted wave (CDW) approximation [31] up to 10 MeV/amu, and by using other less sophisticated methods [32-34]. For $\sigma_{CX}^{(n)}$, CDW data are also given in [35]. The most accurate of these calculations are those of Refs. [25,26] for low energies, Refs. [27,27a,28] for intermediate-to-high energies, and Ref. [31] for the high-energy region. In the energy range of applicability of the employed method, all these calculations have an uncertainty of about 10%, or smaller, at least for the dominant channels. For the electron capture (n,ℓ) channels having small cross sections, the accuracy is not expected to be so high. The cross section results from these references have been taken as a basis for constructing the $\sigma_{CX}^{(n,\ell)}$ cross sections in the energy region from ~ 80 eV/amu to 10 MeV/amu. Since the energy ranges in which the above calculations been made have a significant overlap (mainly due to validity of AO-CC method with inclusion of pseudo-states in the broad region from ~ 10-200 keV/amu), a smooth connection of the results from different energy regions was possible.

The $\sigma_{CX}^{(n)}$ partial cross sections show the following properties. In the energy region below ~2 keV/amu, $\sigma_{CX}^{(n=3)}$ cross section is dominant, while for E > 2

keV/amu, the cross sections $\sigma_{CX}^{(n=2)}$ and $\sigma_{CX}^{(n=3)}$ have comparable magnitudes and are the largest ones. The cross sections $\sigma_{CX}^{(n)}$ for n=4,5,6,7$\cdots$ rapidly decrease with increasing n (particularly at energies below $\sim$50 keV/amu; for energies above $\sim$ 200 keV/amu this decrease follows the n^{-3} Oppenheimer's rule). The $\sigma_{CX}^{(n=1)}$ cross section is very small: in the region of its maximum at E $\approx$ 100 keV/amu it is of order of magnitude of $10^{-18} cm^2$ and is about an order of magnitude smaller than $\sigma_{CX}^{(n=7)}$, the higher n for which state-selective calculations have been performed.

The $\sigma_{CX}^{(n,\ell)}$ cross sections show a more complex dependence on parameter ℓ for a given n and energy. At very low energies ($\lesssim$1 keV/amu), the maximum populated ℓ -sub-level for a given n is $\ell_m = n-1$. For n =2,3, the dominance of $\sigma_{CX}^{(n,n-1)}$ persists even up to E $\approx$ 300keV/amu. With increasing both the energy and n, however, the maximum of ℓ -distribution of captured electrons (i.e. the ratio $\sigma_{CX}^{(n,\ell)}/\sigma_{CX}^{(n)}$) shifts towards lower ℓ -values (for instance, for n = 4 and 5 $\leq$ E(keV/amu) $\leq$ 100, $\ell_m = n-2$). At sufficiently high energies, the most populated ℓ -sub-level becomes always the $\ell = 0$ level for all n. These findings are consistent with the general features of n- and ℓ- distributions of captured electrons in collisions of H(1s) atoms with multiply changed ions [36].

The constructed cross sections $\sigma_{CX}^{(n,\ell)}$ on the basis of the data from Refs. [25-28,31] (considered to be the best) have been fitted to the following types of analytic expressions, the different form of which reflects the different energy behavior of the cross sections

$$\sigma_{CX}^{(n,\ell)} = \frac{a_1 \exp\left[-(a_2/E)^{a_3}\right]}{1+(E/a_4)^{a_5}+(E/a_6)^{a_7}} \quad \left(\times 10^{-16} cm^2\right) \tag{21}$$

$$\sigma_{CX}^{(n,\ell)} = \frac{a_1 \exp\left[-(a_2/E)^{a_3}\right]}{1+(E/a_4)^{a_5}+(E/a_6)^{a_7}+(E/a_8)^{a_9}} \quad \left(\times 10^{-16} cm^2\right) \tag{22}$$

$$\sigma_{CX}^{(n,\ell)} = \frac{a_1 \exp\left[-(a_2/E)^{a_3}\right]}{1+(E/a_4)^{a_5}+(E/a_6)^{a_7}+(E/a_8)^{a_9}} + \frac{a_{10} \exp\left[-(a_{11}/E)^{a_{12}}\right]}{1+(E/a_{13})^{a_{14}}} \quad \left(\times 10^{-16} cm^2\right) \tag{23}$$

$$\sigma_{CX}^{(n,\ell)} = \frac{a_1 \exp\left[-(a_2/E)^{a_3}\right]}{1+(E/a_4)^{a_5}+(E/a_6)^{a_7}+(E/a_8)^{a_9}} + \frac{a_{10} \exp\left[-(a_{11}/E)^{a_{12}}\right]}{1+(E/a_{13})^{a_{14}}+(E/a_{15})^{a_{16}}} \quad \left(\times 10^{-16} cm^2\right) \tag{24}$$

where collision energy E is expressed in eV/amu, and a_i (i=1-16) are fitting parameters. The values of fitting parameters a_i for $\sigma_{CX}^{(n,\ell)}$ cross sections for n=1 and n=2, and n= 3-6 are given in Table 8, and Table 9-12, respectively. The number of parameters in these tables indicates the used analytic fit expression from those given by Eqs. (21)-(24). We note that $\sigma_{CX}^{(n,\ell)}$ for $n\ell = 6h$ is small, and corresponding values of parameters a_i are not shown in Table 12.

The shell-selective partial cross sections $\sigma_{CX}^{(n)}$, obtained by summing $\sigma_{CX}^{(n,\ell)}$ over ℓ, can also be represented by an analytic fit expression in the same form as Eq. (21-24). The corresponding values of fitting parameters a_i for n = 2-7 are given in Table 13.

For all the above electron capture processes, the available theoretical results and the fitting line for the preferred ("recommended") cross section are displayed in figures 3-28.

The extension of $\sigma_{CX}^{(n)}$ and $\sigma_{CX}^{(n,\ell)}$ data to higher n ($\geq$8) cannot be done because of absence of appropriate scalings. Only in the high-energy region (E $\geq$ 200 keV/amu), the Oppenheimer's n^{-3} rule for $\sigma_{CX}^{(n)}$ is known to be valid [36].

4.2. Capture from H($n_0 \geq 2$) levels

Electron capture in H(2s)+ Li^{3+} collisions has been studied at low collision energies by the Landau-Zener [37] and superpromotion [5,38] models, and at intermediate-to-high energies by the AO-CC [39] and other less accurate models [40]. The total electron capture cross section shows a broad maximum in the energy region 0.5-5 keV/amu of about $10^{-14} cm^2$. For energies below ~0.5-5 keV/amu, dominantly populated final n-shells are n=5 and n=6 ($\sigma_{CX}^{(n=6)}$ is, however, by a factor of two smaller than $\sigma_{CX}^{(n=5)}$), while for E $\geq$ 0.5 keV/amu, n=4 shell is dominantly populated. Within n=4 shell, the 4f state is dominantly populated up to E$\approx$5 keV/amu and then its population becomes comparable with that of 4d. Within n= 5, dominantly populated state is 5f for energies below ~10 keV/amu.

The state-selective electron capture cross sections for H(2p)+Li^{3+} collisions have been calculated only by the AO-CC method [39]. The cross section magnitude and relative importance of individual final (capture) channels are

similar as in the case of $H(2s)+Li^{3+}$ case.

For $n_0 \geq 2$, total electron capture cross section calculations are available (for selected n_0 between $n_0 = 2$ and $n_0 = 20$) from the CTMC calculations of Ref. [41] (for q = 2) and Ref. [42] (q = 5,10). These data, together with the experimental data on $H(n_0) + He^{2+}$ collision system ($n_0 = 8$-24) [43], have been represented in Ref. [44] in a compact, scaled form (within an uncertainty of 10-30%)

$$\tilde{\sigma}_{CX}^{tot}(q) \equiv \frac{\sigma_{CX}^{tot}(n_0)}{q n_0^4} = 7.04 \frac{a}{\tilde{E}^{3.5}\left(1+b\tilde{E}^2\right)}\left\{1-\exp\left[-\frac{2\tilde{E}^{3.5}\left(1+b\tilde{E}^2\right)}{3a}\right]\right\} \quad \left(\times 10^{-16} cm^2\right) \qquad (25)$$

where $\tilde{E} = E n_0^2 / q^{0.5}$ (keV/amu), $a = 1.507 \times 10^5$, $b = 1.974 \times 10^{-5}$.

Below $\tilde{E} \sim 10$ keV/amu, the energy dependence of σ_{CX}^{tot} is very weak, and for $\tilde{E} \to 0$, $\tilde{\sigma}_{CX}^{tot} = 1.06 \times 10^{-15} cm^2$. The experimental data of Ref. [43] for $H(n_0 \geq 8) + He^{2+}$, represented by Eq. (25) with an accuracy of $\sim 20\%$, extend down to $\tilde{E} \approx 10$ keV/amu. For the partial cross sections $\sigma_{CX}^{(n)}(n_0)$ and $\sigma_{CX}^{(n,\ell)}(n_0)$ with $n_0 \geq 3$ neither direct calculations nor scaling relationships are available. From the general theory of charge exchange reactions of one-electron systems with multiply charged ions [36] it follows that dominantly populated n-shell of $Li^{2+}(n)$ at energies below $\sim 1/n_0$ keV/amu should be [36]

$$n_m \cong 2^{1/4} n_0 q^{3/4} \cong 2.71 n_0 \qquad (26)$$

5. Conclusions

In the present report we have compiled and critically assessed the available cross section information on collision processes of Li^{3+} ions with atomic hydrogen. The processes include excitation, ionization and charge exchange from the ground and excited hydrogen levels. The energy range considered extends from ~ 100eV/amu to the MeV/amu region.

The cross section information on these processes found in literature pertains mostly to H in its ground state. For the processes involving excited initial states it is either sparse (the case of charge exchange) or completely missing

(for excitation and ionization). Therefore, certain well established cross section scaling relationships had to be employed to generate the missing cross section information.

In the case of charge exchange process from H(1s), capture to specific states of Li^{2+} ($n\ell$) ion has been also considered in view of its importance for plasma charge exchange recombination diagnostics.

The critically assessed cross sections for above processes have been represented by relatively simple analytic fit functions. These fit functions have been chosen to have correct physical behavior at both low and high energies and can ensure reliable extrapolations. The error of the analytic fits to the cross sections is well within the uncertainty of original data.

Although the present database can usefully serve the needs for Li^{3+} -based plasma diagnostics, its completion with the presently missing cross sections (especially for electron capture from excited H($n \geq 2$) levels) is highly desirable.

References

1. K. Khlopenkov, S. Sudo, Plasma Phys. Control. Fusion 43 (2001) 1547.
2. S. Sudo et al., Plasma Phys. Control. Fusion 44 (2002) 129.
3. J. N. Brooks, T. Rognlien, D. N. Ruzic et al., J. Nucl. Materials 185 (2001) 290.
4. J. P. Allain, M. Nieto, M. D. Coventry et al., Fusion Eng. & Design, 61-62 (2002) 245.
5. R. K. Janev, E. A. Solov'ev, Yi Wang, J. Phys. B 29 (1996) 2497.
6. B. H. Bransden, C. J. Noble, J. Phys. B 15 (1982) 451.
7. C. O. Reinbold, R. E. Olson, W. Fritsch, Phys. Rev. A 41 (1990) 4837.
8. W. Fritsch, Proc. 6th Int. Conf. Phys. Highly Charged Ions, (Eds. P. Richard et al., AIP Conf. Proc. 274 N. Y., 1993) p. 24.
9. P. S. Krstic, R. K. Janev, Phys. Rev. A 47 (1993) 3894.
10. P. S. Krstic, M. Radmilovic, R. K. Janev, At. Plasma-Mater. Int. Data Fusion 3 (1992) 113.
11. R. K. Janev, J. J. Smith, At. Plasma-Mater. Int. Data Fusion 4 (1993) 1.
12. E. A. Solov'ev, J. A. Stephens, R. K. Janev, At. Plasma-Mater. Int. Data Fusion 9 (2001) 132.

13. J. G. Lodge, I. C. Percival, D. Richards, J. Phys. B 9 (1976) 239.
14. M. B. Shah, T. V. Goffe, H. B. Gilbody, J. Phys. B 11 (1978) L233.
15. M. B. Shah, H. B. Gilbody, J. Phys. B 15 (1982) 3441.
16. N. Toshima, Phys. Rev. A 50 (1994) 3940.
17. L. F. Errea, C. Harel, C. Illescas et al., J. Phys. B 31 (1998) 3199.
18. C. Illescas, A. Riera, Phys. Rev. A 60 (1999) 4546.
19. D. S. F. Crothers, J. F. McCann, J. Phys. B 16 (1983) 3229.
20. G. H. Gillespie, J.Phys. B 15 (1982) L729.
21. R. K. Janev, G. Ivanovski, E. A. Solov'ev, Phys. Rev. A 49 (1994) 645.
22. R. K. Janev, L. P. Presnyakov, J. Phys. B 13 (1980) 4233.
23. R. K. Janev, Phys. Rev. A 28 (1983) 1810.
24. W. Seim, A. Müller, I. Wirkner-Bott, E. Solzborn, J. Phys. B 14 (1981) 3475.
25. M. Kimura, private communication (2001).
26. C. Harel, H. Jouin, B. Pons, At. Data Nucl. Tables, 68 (1998) 279.
27. N. Toshima, H. Tawara, NIFS-DATA 26 (1995).
27a. N.Toshima, Phys. Scripta T73 (1997) 144.
28. W. Fritsch, C. D. Lin, J. Phys. B 45 (1982) L281.
29. R. E. Olson, Phys. Rev. A 24 (1981) 1726.
30. E. O. Alt, G. V. Avakov, L. D. Blokhintsev et al., J. Phys. B 13 (1980) 4245.
31. D. S. Belkic, R. Gayet, A. Salin, At. Data Nucl. Tables, 51 (1992) 59.
32. C. R. Mandal, S. Datta, S. C. Mukherjee, Phys. Rev. A 24 (1981) 3044.
33. S. Datta, C. R. Mandal, S. C. Mukherjee, N. C. Sil, Phys. Rev. A 26 (1982) 2551.
34. K. E. Banyard, G. W. Shirtcliffe, Phys. Rev. A 30 (1984) 604.
35. D. S. F. Crothers, J. Phys. B 14 (1981) 1035.
36. R. K. Janev, L. P. Presnyakov, V. B. Shevelko, "Physics of Highly Charged Ions" (Springer-Verlag, Berlin-Heidelberg, 1985).
37. J. I. Casaubon, R. D. Piacentini, J. Phys. B 17 (1984) 1623.
38. E. A. Solov'ev, J. A. Stephens, R. K. Janev, At. Plasma-Mater. Int. Data Fusion (IAEA), 9 (2001) 132; also in :IAEA NDS Report: INDC (NDS) 393 (1999).
39. N. Toshima, C. D. Lin, Phys. Rev. A 47 (1993) 4831.
40. C. C. Montanavi, M. S. Gravielle, J. E. Miraglia, Physica Scripta 56 (1997) 279.
41. D. R. Schultz, L. Meng, C. O. Reinhold, R. E. Olson, Physica Scripta T37

(1991) 89.
42. R. E. Olson, J. Phys. B 13 (1980) 483.
43. M. Burniaux, F. Brouillard, A. Jognaux et al., J. Phys. B 10 (1977) 2421.
44. R. K. Janev, Phys. Lett. A 160 (1991) 67.
45. D. S. Belkic, Phys. Scripta 43 (1991)561.

Table 1. Values of parameters a_i in Eq. (5) for excitation of n = 2,3,4 levels

a_i	n=2	n=3	n=4
a_1	4.84520(+2)*	5.04618(+1)	1.59325(+1)
a_2	6.69602(+1)	8.21366(+1)	7.94188(+1)
a_3	2.78499(-2)	4.50894(-1)	8.82429(-1)
a_4	1.01627(-5)	7.06132(-6)	6.52302(-6)
a_5	4.84603(-3)	5.16969(-1)	4.46519(-1)
a_6	-3.19529(+0)	-4.17842(+0)	-4.24975(+0)
a_7	3.36324(-2)	1.67102(-1)	4.12196(-2)
a_8	2.64997(+1)	2.87789(+1)	2.28376(+1)
a_9	9.56579(-4)	1.59714(-4)	1.58302(-8)
a_{10}	3.84978(+0)	4.77936(+0)	8.74347(+0)

* $a(\pm x) = a \times 10^{\pm x}$

Table 2. Values of fitting parameters b_i in Eq. (6) for excitation of n = 5,6 levels

b_i	n=5	n=6
b_1	1.1204(+1)*	5.7394(+0)
b_2	9.6873(+1)	1.1152(+2)
b_3	7.0587(-2)	1.3088(-1)
b_4	7.2281(-5)	8.8253(-5)
b_5	1.0354(-1)	8.5857(-2)
b_6	-2.4161(+0)	-2.2905(+0)
b_7	1.9046(+0)	1.9145(+0)
b_8	-6.3726(+0)	-5.5986(+0)

* $a(\pm x) = a \times 10^{\pm x}$

Table 3. Values of parameters c_i in Eq. (8) for the excitation transition of $n_0 = 2 \rightarrow n = 3,4,5$

c_i	n=2	n=3	n=4
c_1	3.95830(+3)*	5.26643(+2)	1.73597(+2)
c_2	4.67919(+1)	5.18702(+1)	5.69191(+1)
c_3	1.72288(−1)	6.21216(−1)	9.68539(−1)
c_4	1.42039(−3)	7.86601(−4)	9.00919(−4)
c_5	1.08533(−1)	1.17296(−1)	1.05702(−1)
c_6	−1.22181(+0)	−1.56016(+0)	−1.47750(+0)

* $a(\pm x) = a \times 10^{\pm x}$

Table 4. Values of coefficients c_{2-n} in Eq. (9) for excitation transition of $2 \rightarrow n(n = 6,7,8,9,10)$

n	n=6	n=7	n=8	n=9	n=10
c_{2-n}	0.4610	0.2475	0.1465	0.0920	0.0605

Table 5. Values of fitting parameters c_i in Eq. (8) for $n_0 = 3 \rightarrow n = 4,5,6$ excitation transitions

c_i	n=4	n=5	n=6
c_1	1.16987(+4)*	1.78730(+3)	5.95331(+2)
c_2	3.39570(+1)	3.32880(+1)	3.45210(+1)
c_3	8.74514(−1)	9.69935(−1)	1.44722(+0)
c_4	5.66708(−3)	5.92691(−3)	6.31140(−3)
c_5	1.73728(−1)	1.80588(−1)	1.78202(−1)
c_6	−1.27220(+0)	−1.28940(+0)	−1.28810(+0)

* $a(\pm x) = a \times 10^{\pm x}$

Table 6. Values of coefficients c_{3-n} in Eq. (11) for excitation transitions $3 \rightarrow n(n = 7-10)$

n	n=7	n=8	n=9	n=10
c_{3-n}	0.4670	0.2545	0.1540	0.1000

Table 7. Values of fitting parameters a_i in Eq. (15) for ionization cross section of H(n_0), n = 1,2,3 by Li^{3+} impact

a_i	n_0=1	n_0=2	n_0=3
a_1	8.30194(+1)*	1.66484(+2)	7.53658(+2)
a_2	1.15973(+2)	5.19714(+1)	1.92724(+1)
a_3	2.77580(+7)	4.52808(+21)	1.83610(+9)
a_4	4.59930(-6)	2.16126(-3)	4.93943(-2)
a_5	1.91247(-2)	4.74902(-2)	1.36404(-1)
a_6	-3.57909(+0)	-2.41416(+0)	-1.16090(+0)
a_7	6.29546(-2)	1.60611(-3)	1.30281(+0)
a_8	-1.62357(+0)	3.88616(-2)	-2.77601(+0)

* $a(\pm x) = a \times 10^{\pm x}$

Table 8. Values of fitting parameters a_i for $\sigma_{CX}^{(n,\ell)}$ in Eq. (23) for $n = 1$ and in Eq. (22) for n=2

a_i	1s	2s	2p
a_1	8.5833(-1)	1.0795(+3)	1.8660(+3)
a_2	1.0919(+6)	1.2027(+6)	1.2061(+6)
a_3	4.6504(-1)	2.9973(-1)	2.9785(-1)
a_4	2.9509(+4)	4.1258(+3)	1.5605(+3)
a_5	-2.1907(+0)	1.7088(+0)	8.6085(-1)
a_6	9.5881(+4)	9.3273(+3)	1.6528(+4)
a_7	3.1259(+0)	3.1257(+0)	3.4454(+0)
a_8	2.4012(+5)	4.9259(+4)	5.3094(+4)
a_9	5.6032(+0)	5.6066(+0)	6.1615(+0)
a_{10}	1.6874(+1)		
a_{11}	1.3618(+4)		
a_{12}	6.7598(-1)		
a_{13}	2.1373(+1)		
a_{14}	3.5534(+0)		

* $a(\pm x) = a \times 10^{\pm x}$

Table 9. Values of fitting parameters a_i for $\sigma_{CX}^{(n,\ell)}$ in Eq. (22) for 3s and 3p, and in Eq. (23) 3d

a_i	3s	3p	3d
a_1	1.2501(+1)	2.3666(+1)	2.2209(+1)
a_2	2.9346(+6)	2.0288(+6)	1.8692(+4)
a_3	1.5702(-1)	1.5563(-1)	5.5415(-1)
a_4	5.3156(+4)	5.9278(+4)	5.7957(+4)
a_5	4.3742(+0)	4.5574(+0)	6.0668(+0)
a_6	1.7553(+4)	4.1115(+4)	2.9885(+4)
a_7	2.1353(+0)	2.5256(+0)	3.4442(+0)
a_8	1.1964(+5)	9.7507(+4)	9.7442(+4)
a_9	5.9502(+0)	6.1913(+0)	5.9651(+0)
a_{10}			6.0765(+0)
a_{11}			2.1264(+3)
a_{12}			2.7457(-1)
a_{13}			1.0146(+3)
a_{14}			3.2956(+0)

* $a(\pm x) = a \times 10^{\pm x}$

Table 10. Values of fitting parameters a_i in Eq. (24) for $\sigma_{CX}^{(n,\ell)}$ for $n = 4$

a_i	4s	4p	4d	4f
a_1	1.9807(+0)	5.8172(+0)	6.8352(+0)	2.6988(+0)
a_2	3.0693(+5)	3.0879(+5)	3.0879(+5)	3.0879(+5)
a_3	3.1672(-1)	3.3179(-1)	3.2622(-1)	3.1213(-1)
a_4	7.8964(+4)	7.7848(+4)	7.7853(+4)	7.7831(+4)
a_5	3.3043(+0)	4.2739(+0)	3.0443(+0)	5.8111(+0)
a_6	3.9049(+4)	6.4526(+4)	6.4635(+4)	6.4459(+4)
a_7	2.8297(+0)	4.0548(+0)	5.5804(+0)	6.0667(+0)
a_8	8.7775(+4)	9.5977(+4)	9.5968(+4)	9.5973(+4)
a_9	5.4039(+0)	6.1357(+0)	6.4213(+0)	1.9245(+0)
a_{10}	1.7856(+2)	2.7492(-1)	9.8665(-1)	5.2029(-1)
a_{11}	5.0490(+3)	4.8559(+3)	4.8536(+3)	4.8690(+3)
a_{12}	3.0792(+0)	1.2215(+0)	1.3517(+0)	7.2433(-1)
a_{13}	1.0748(+3)	1.7250(+3)	1.7210(+4)	1.6908(+3)
a_{14}	1.3623(+1)	1.1163(+0)	1.7927(+0)	6.5445(-1)
a_{15}	7.5998(+3)	7.5993(+3)	7.5989(+3)	7.6791(+3)
a_{16}	5.9852(+0)	4.2605(+1)	5.2865(+1)	4.0681(+0)

* $a(\pm x) = a \times 10^{\pm x}$

Table 11. Values of fitting parameters a_i in Eq. (24) for $\sigma_{CX}^{(n,\ell)}$ for $n=5$

a_i	5s	5p	5d	5f	5g
a_1	2.9589(+4)	2.9610(+4)	2.9560(+4)	2.9551(+4)	2.9588(+4)
a_2	8.6902(+5)	8.6902(+5)	8.6902(+5)	8.6902(+5)	8.6902(+5)
a_3	4.7454(-1)	5.1531(-1)	4.3330(-1)	4.2289(-1)	4.5340(-1)
a_4	6.1427(+3)	6.1425(+3)	6.1423(+3)	6.1423(+3)	6.1427(+3)
a_5	5.8954(-1)	1.1564(+0)	8.5495(-1)	1.5005(+0)	6.5271(-2)
a_6	6.4719(+2)	5.9453(+2)	7.4504(+1)	1.0527(+2)	8.0194(+2)
a_7	2.3567(+0)	1.4956(+0)	1.2092(+0)	1.5162(+0)	2.6179(+0)
a_8	1.9494(+4)	1.9694(+4)	1.9219(+4)	1.9136(+4)	1.9467(+4)
a_9	5.8919(+0)	6.0080(+0)	6.2439(+0)	6.7015(+0)	7.5035(+0)
a_{10}	8.8685(-2)	9.2030(-2)	4.3839(-2)	3.1062(-2)	7.2181(-2)
a_{11}	4.1267(+4)	4.1269(+4)	4.1287(+4)	4.1283(+4)	4.1271(+4)
a_{12}	4.0393(-1)	3.3759(-1)	4.1175(-1)	3.9622(-1)	4.0936(-1)
a_{13}	1.1251(+3)	1.3872(+3)	1.1241(+4)	1.1240(+4)	1.1255(+4)
a_{14}	-5.5447(-1)	-1.9538(+0)	2.0048(+0)	2.2867(+0)	2.3253(+0)
a_{15}	6.1107(+4)	6.1108(+4)	6.1148(+4)	6.1149(+4)	6.1124(+4)
a_{16}	4.7226(+0)	5.8212(+0)	5.2734(+0)	5.0499(+0)	5.4616(+0)

* $a(\pm x) = a\times 10^{\pm x}$

Table 12. Values of fitting parameters a_i in Eq. (21) for $\sigma_{CX}^{(n,\ell)}$ for $n=6$
($\sigma_{CX}^{(n,\ell)}$ for $n\ell = 6h$ is small and not shown here)

a_i	6s	6p	6d	6f	6g
a_1	2.8852(+5)*	4.1604(+5)	2.5759(+4)	2.5605(+4)	2.2209(+4)
a_2	7.6028(+5)	1.1919(+6)	1.1456(+5)	4.4935(+5)	2.6385(+5)
a_3	6.4890(−1)	5.8398(−1)	9.5729(−1)	7.4489(−1)	8.3042(−1)
a_4	5.0200(+3)	4.5375(+3)	1.6186(+2)	9.4048(+3)	8.9336(+3)
a_5	4.3527(+0)	3.2608(+0)	1.6786(+0)	4.0746(+0)	5.7968(+0)
a_6	1.1099(+4)	1.6024(+4)	1.3463(+4)	1.2281(+4)	1.6229(+4)
a_7	5.7395(+0)	6.3637(+0)	5.9743(+0)	5.9934(+0)	5.8128(+0)

* $a(\pm x) = a\times 10^{\pm x}$

Table 13. Values of fitting parameters a_i in Eq. (21-24) but for n-selective cross sections $\sigma_{CX}^{(n,\lambda)}$, for $n = 2$-7

a_i	2	3	4	5	6	7
a_1	3.2285(+3)	4.5013(+5)	2.7945(+1)	3.9605(+4)	1.0645(+0)	6.8054(+4)
a_2	1.2032(+6)	6.0007(-3)	3.0879(+5)	8.6902(+5)	5.9413(+4)	8.4908(+5)
a_3	2.9923(-1)	-1.5258(-1)	3.2323(-1)	4.6249(-1)	5.1555(-1)	4.8405(−1)
a_4	2.4583(+3)	1.3138(+4)	7.7827(+4)	6.1422(+3)	7.9956(+4)	3.3952(+2)
a_5	1.2528(+0)	-3.4971(+0)	3.9735(+0)	1.2053(+0)	4.4936(+0)	1.7087(+0)
a_6	1.8499(+4)	7.2544(+4)	6.4553(+4)	4.6778(+2)	1.0236(+5)	1.6477(+4)
a_7	3.9143(+0)	2.5157(+0)	5.5443(+0)	1.4458(+0)	5.7539(+0)	5.8670(+0)
a_8	4.8151(+4)	2.1012(+4)	9.5977(+4)	1.9698(+4)		
a_9	5.7723(+0)	-1.3108(+0)	1.6934(-1)	5.7783(+0)		
a_{10}		1.4577(+1)	3.8125(+0)	3.0066(-1)		
a_{11}		1.8457(+5)	4.8562(+3)	4.1268(+4)		
a_{12}		1.3262(-1)	1.1121(+0)	3.2486(-1)		
a_{13}		4.4535(+3)	1.7255(+3)	1.3114(+3)		
a_{14}		3.5393(+0)	2.0477(+0)	-1.9767(+0)		
a_{15}			7.6001(+3)	6.1110(+4)		
a_{16}			1.8493(+1)	5.6313(+0)		

* $a(\pm x) = a \times 10^{\pm x}$

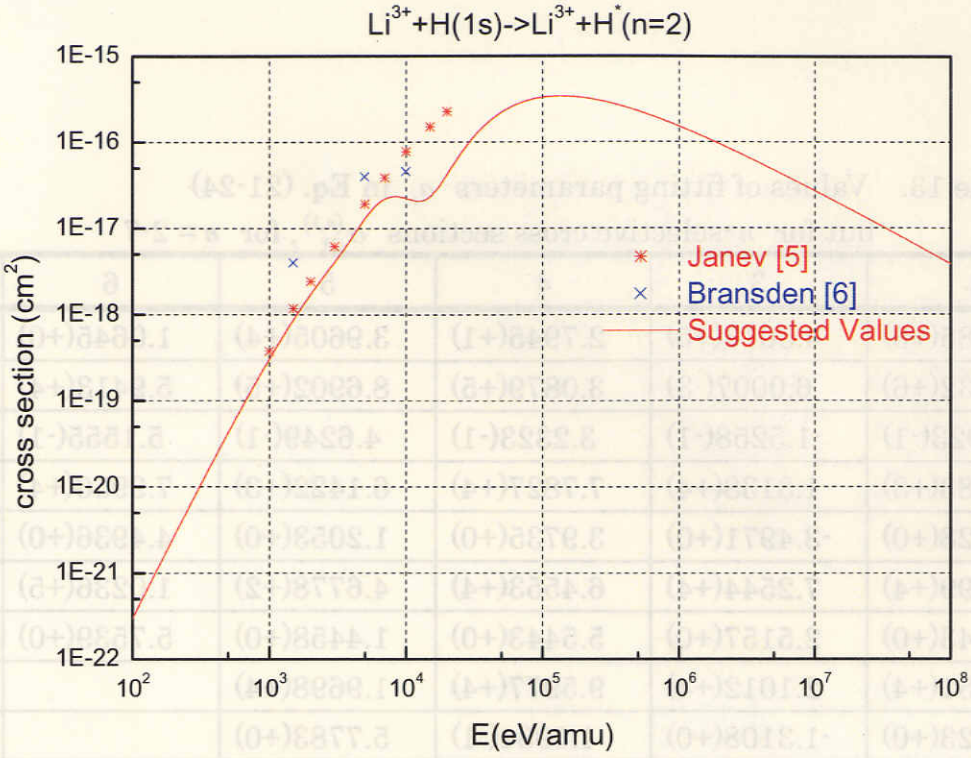

Figure 1. Preferred (full line; see text) cross section for excitation of H(n=2) by Li^{3+} colliding with H(1s).

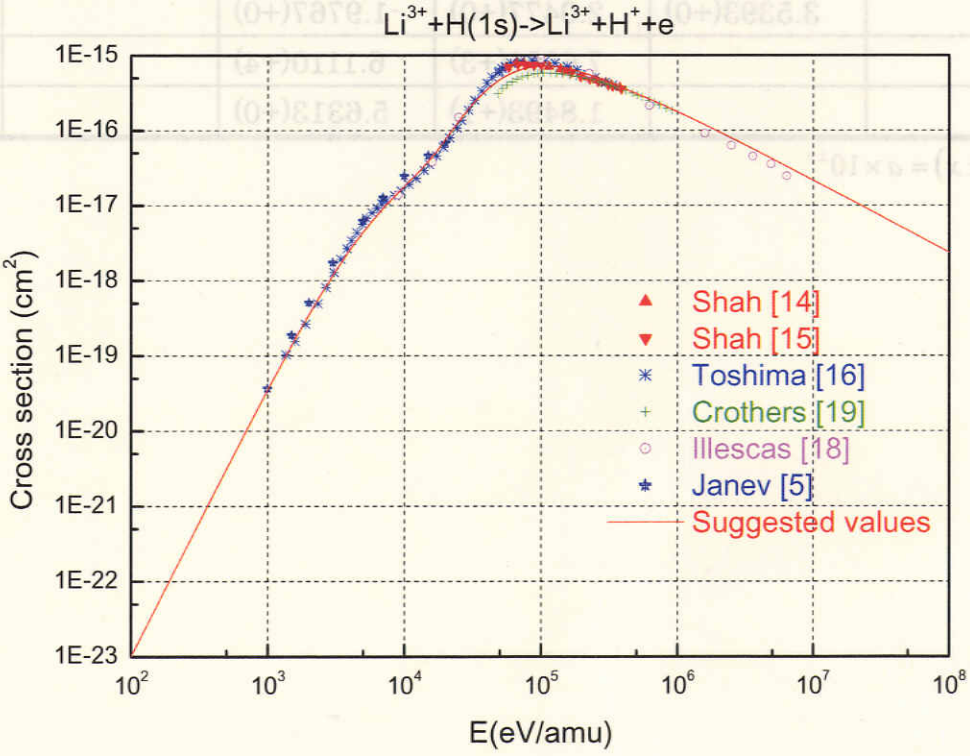

Figure 2. Fit (full line) of preferred ionization cross section of H(1s) by Li^{3+} impact.

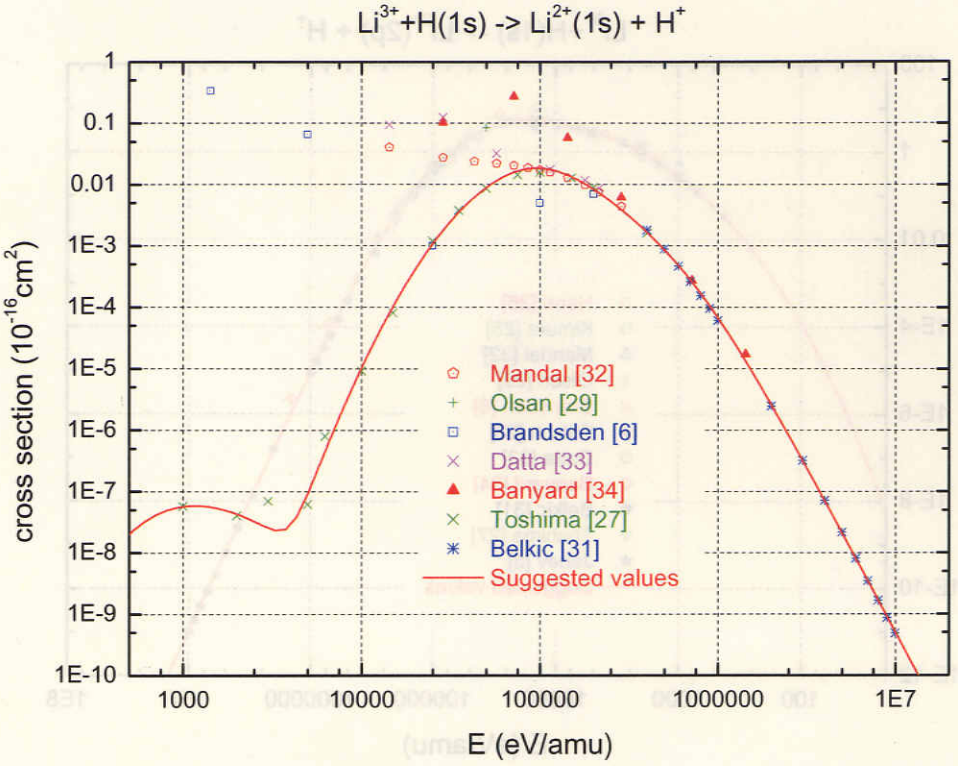

Figure 3. Fit (full line) of preferred electron capture cross section to $Li^{2+}(1s)$ in collisions of Li^{3+} with H(1s).

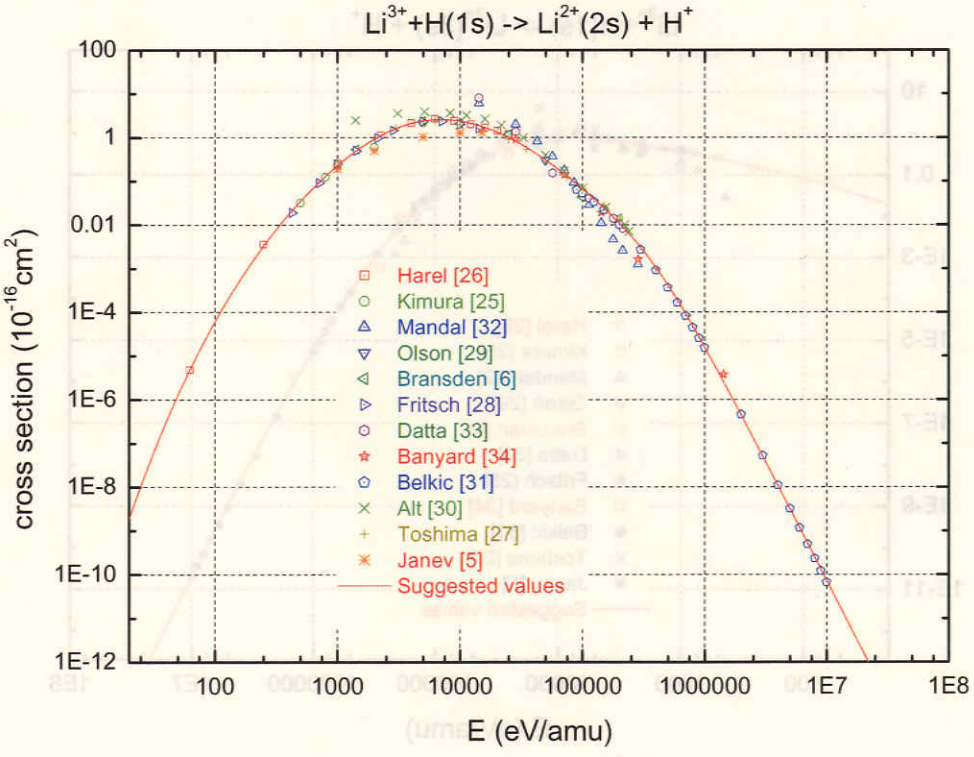

Figure 4. Same as in Fig.3, but for capture to $Li^{2+}(2s)$.

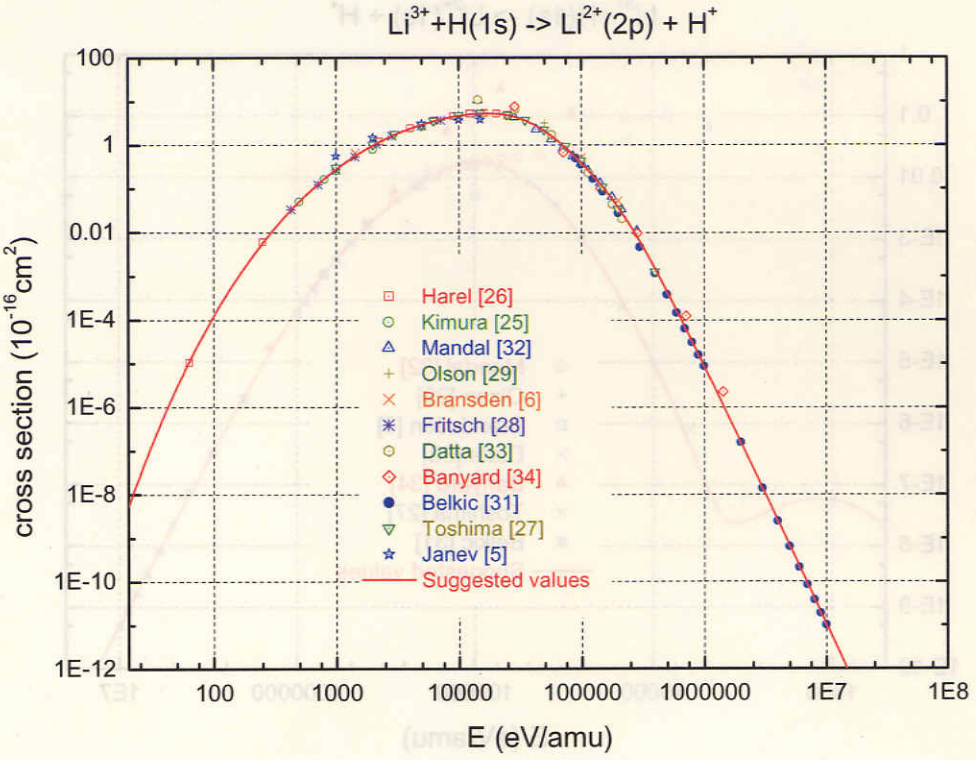

Figure 5. Same as in Fig.3, but for capture to $Li^{2+}(2p)$.

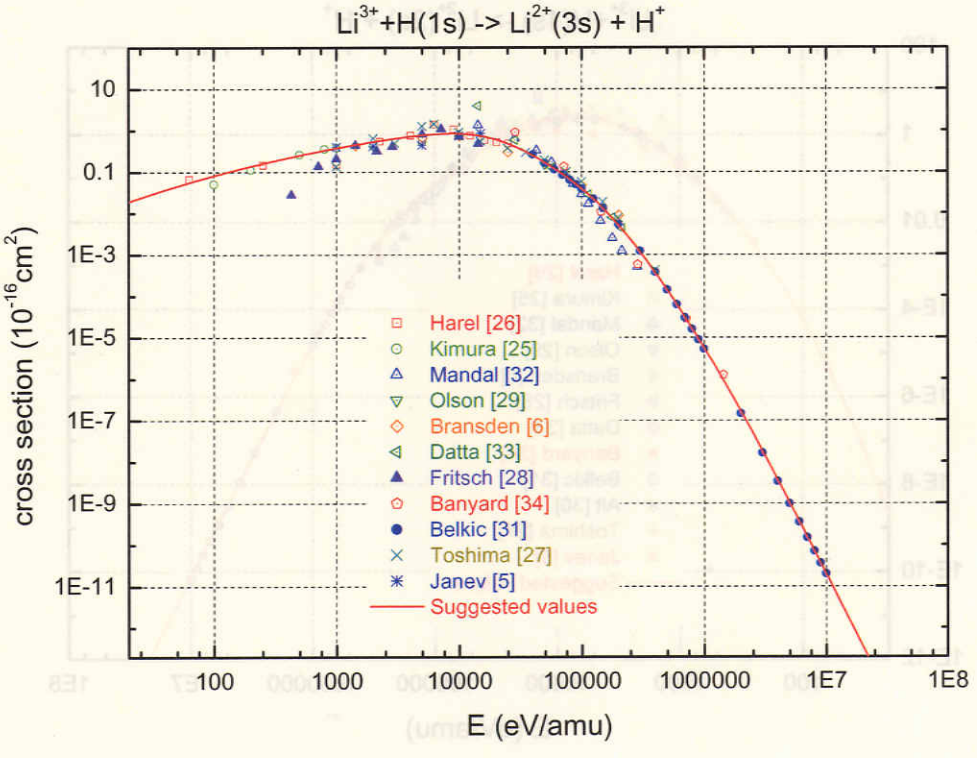

Figure 6. Same as in Fig.3, but for capture to $Li^{2+}(3s)$.

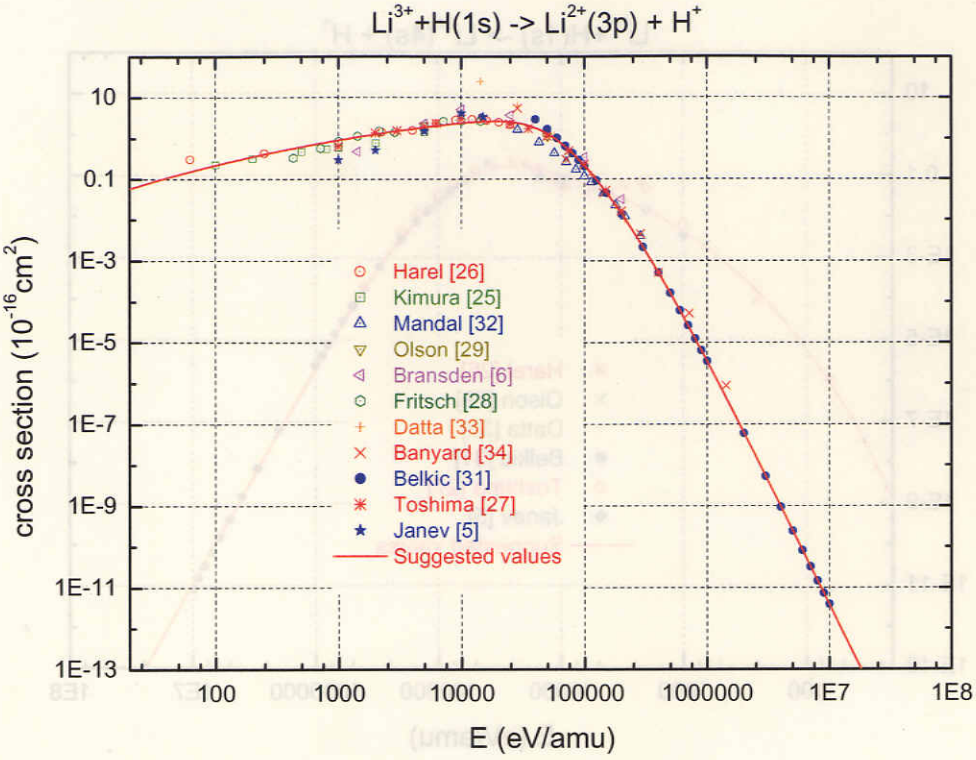

Figure 7. Same as in Fig.3, but for capture to $Li^{2+}(3p)$.

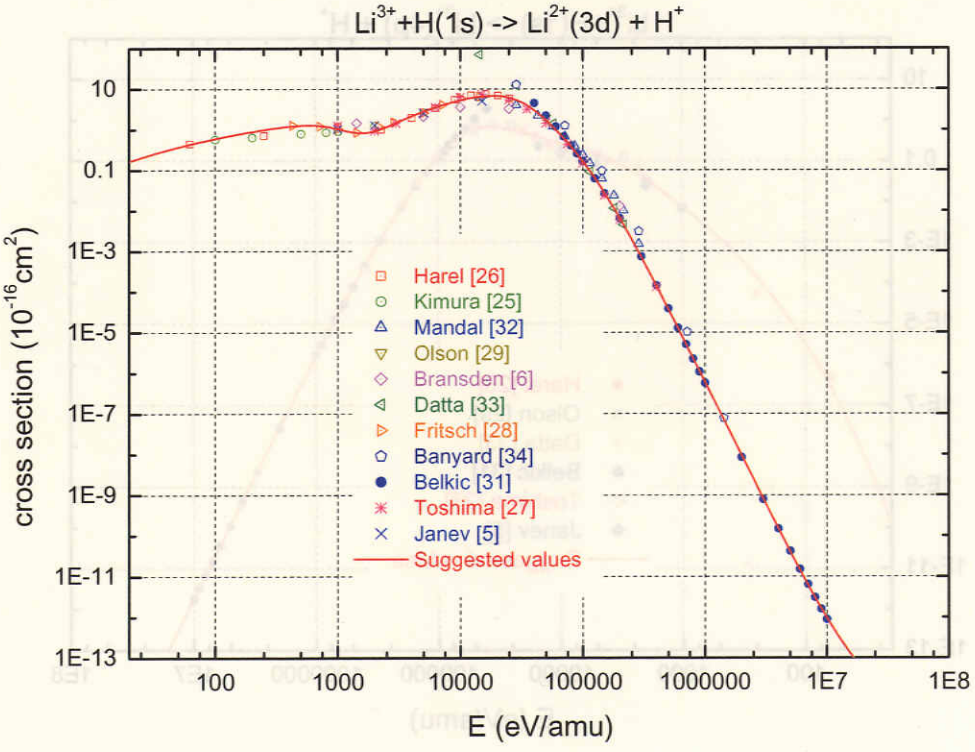

Figure 8. Same as in Fig.3, but for capture to $Li^{2+}(3d)$.

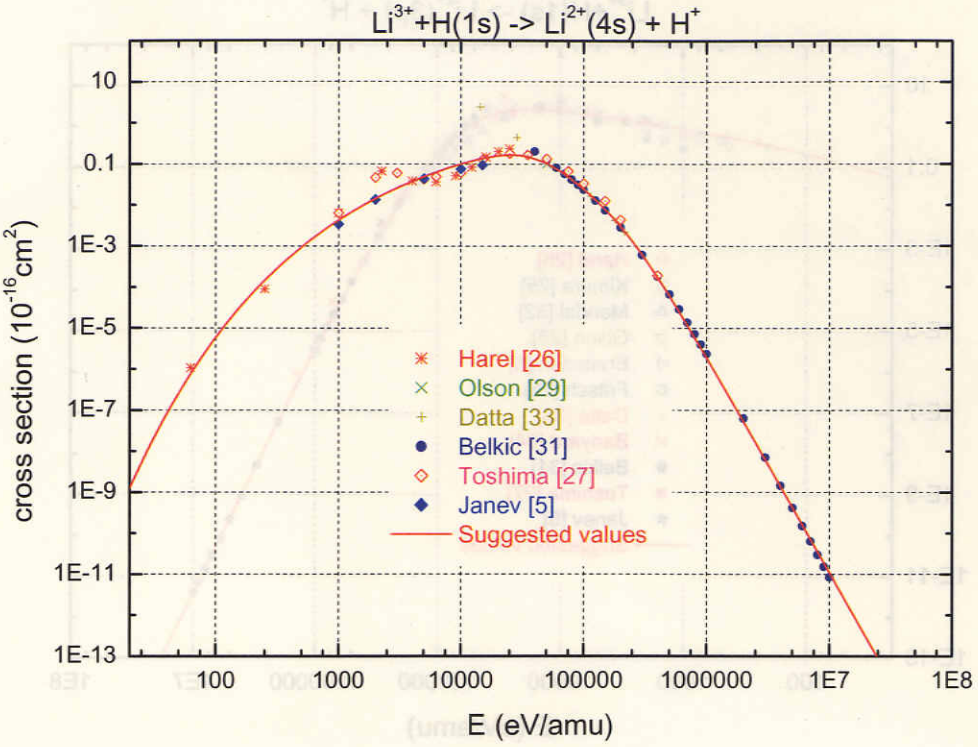

Figure 9. Same as in Fig.3, but for capture to $Li^{2+}(4s)$.

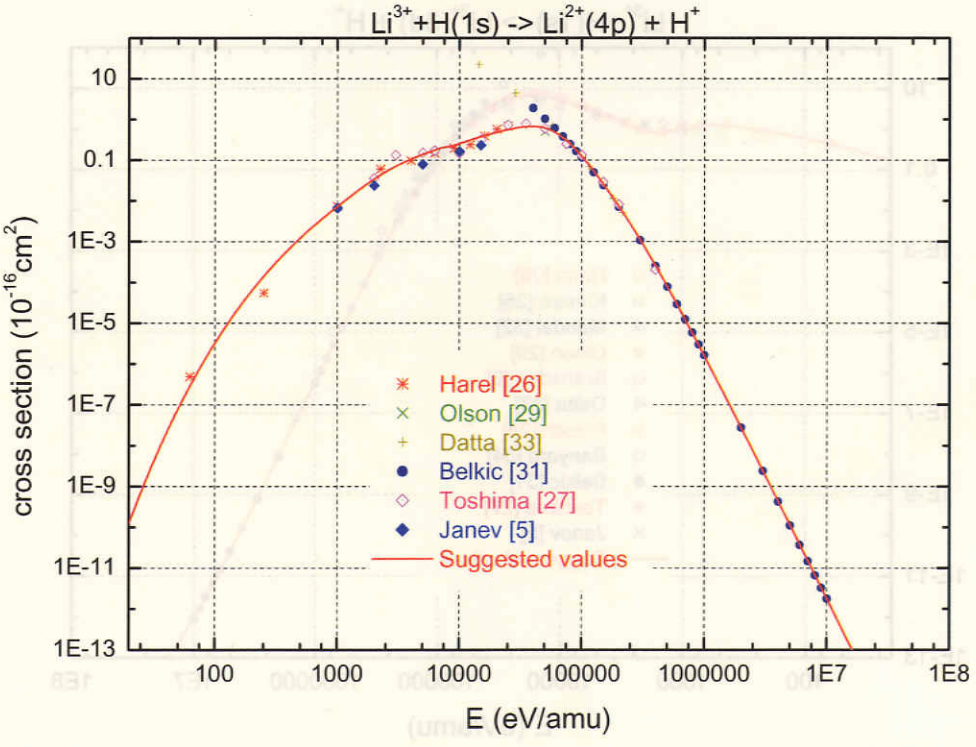

Figure 10. Same as in Fig.3, but for capture to $Li^{2+}(4p)$

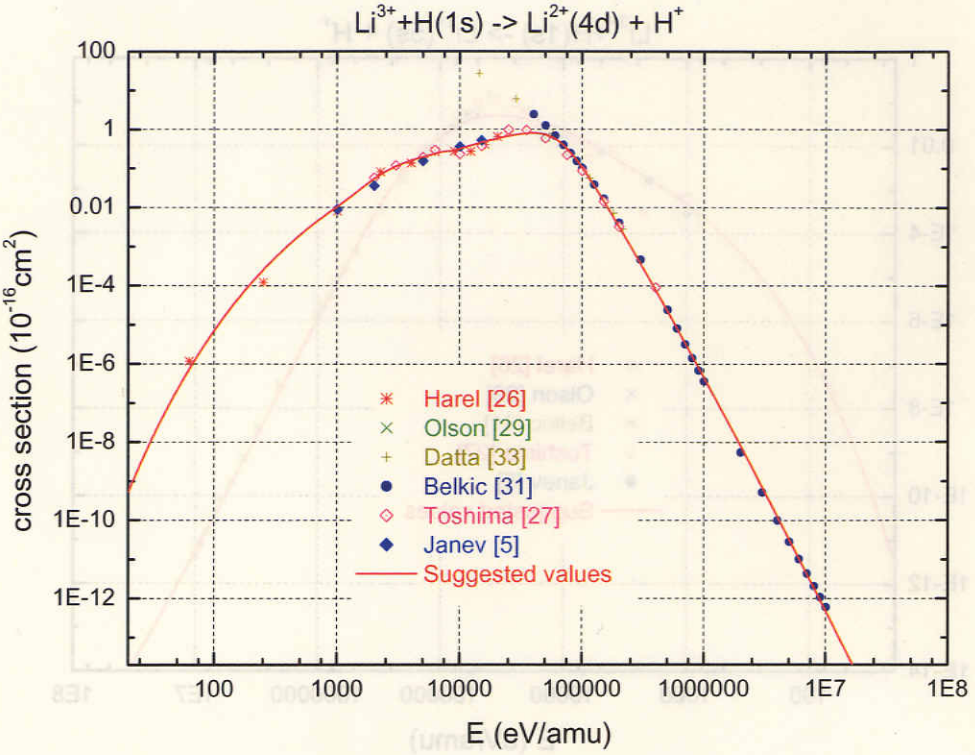

Figure11. Same as in Fig.3, but for capture to $Li^{2+}(4d)$.

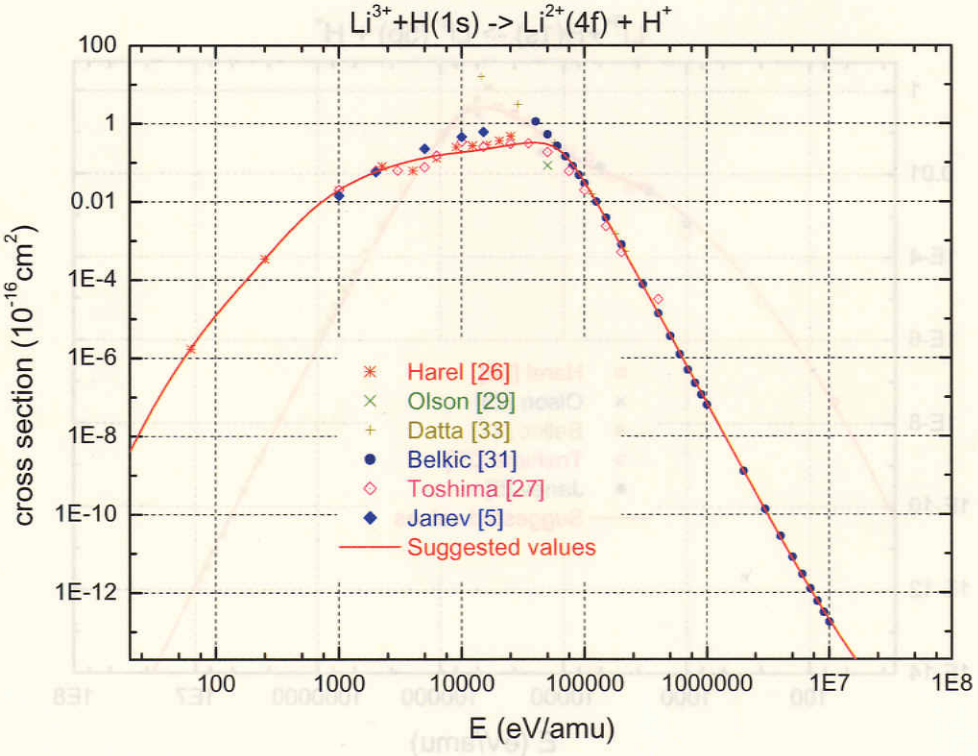

Figure 12. Same as in Fig.3, but for capture to $Li^{2+}(4f)$.

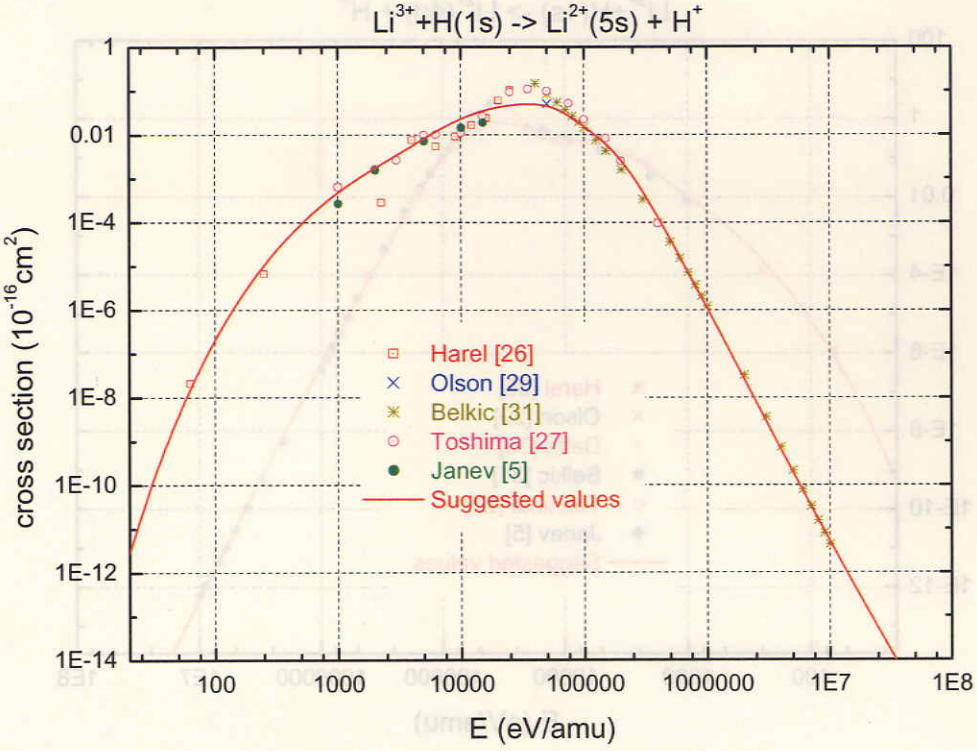

Figure 13. Same as in Fig.3, but for capture to $Li^{2+}(5s)$.

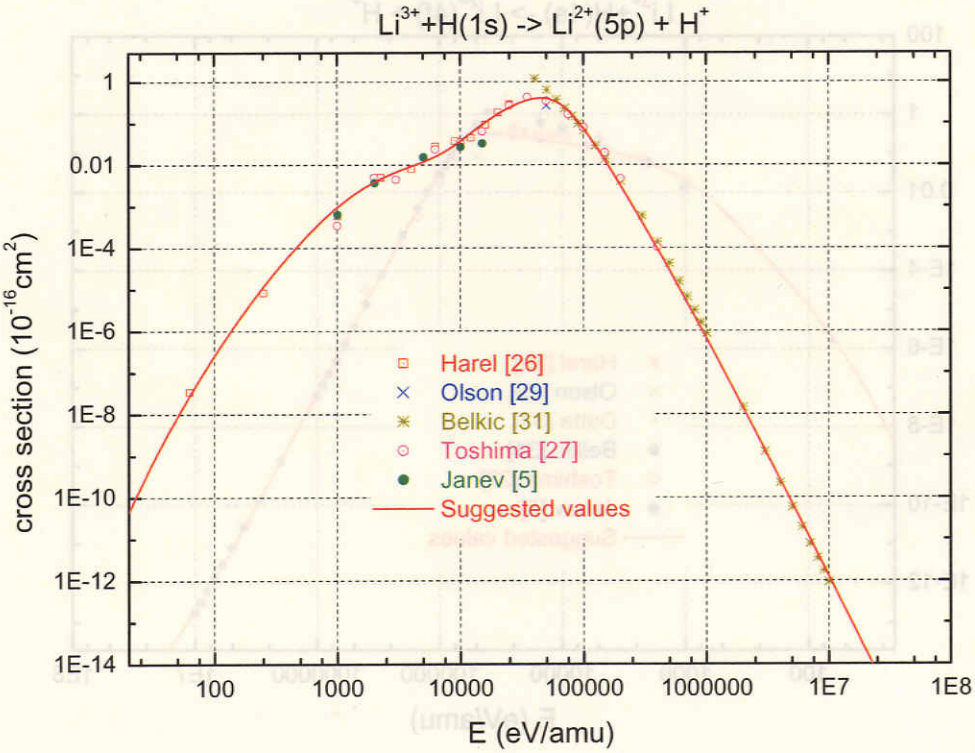

Figure 14. Same as in Fig.3, but for capture to $Li^{2+}(5p)$.

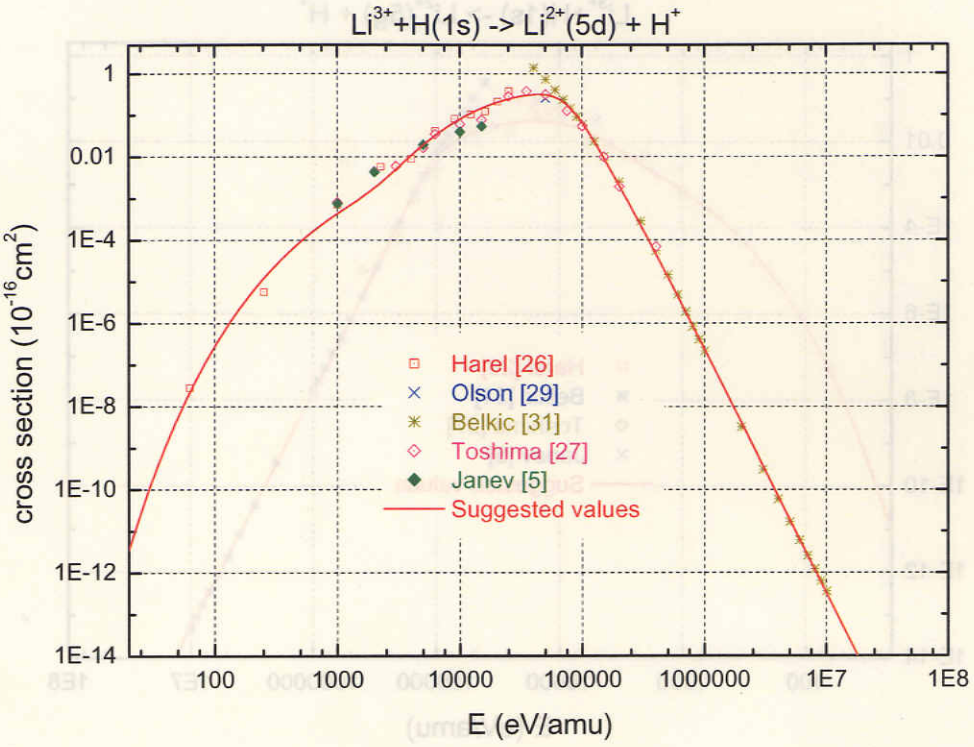

Figure 15. Same as in Fig.3, but for capture to $Li^{2+}(5d)$.

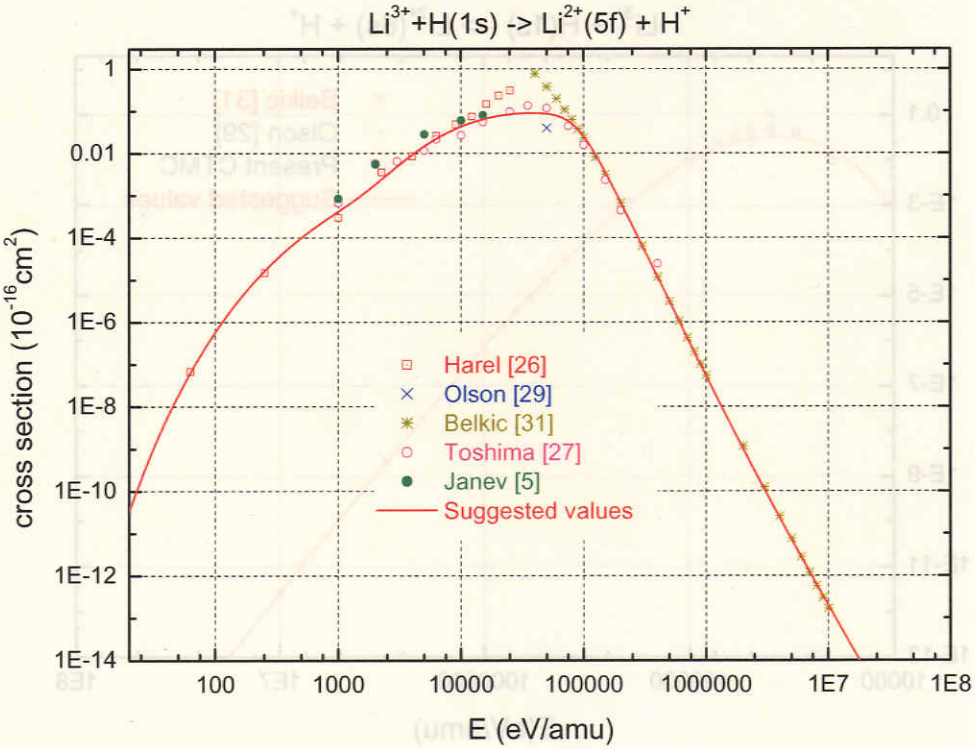

Figure 16. Same as in Fig.3, but for capture to $Li^{2+}(5f)$.

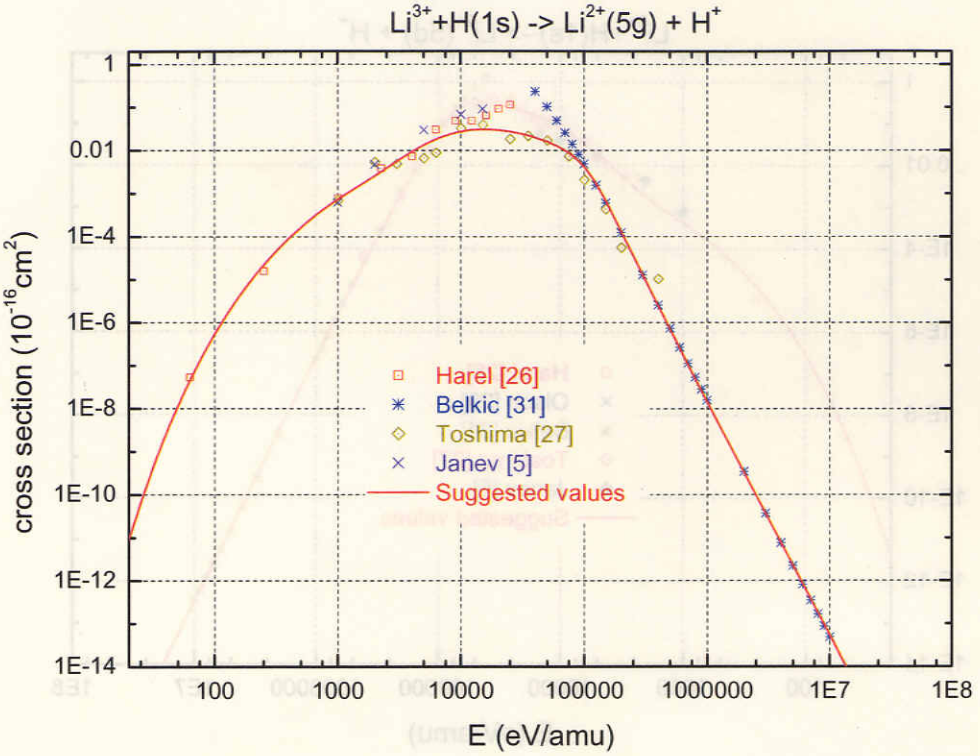

Figure 17. Same as in Fig.3, but for capture to $Li^{2+}(5g)$.

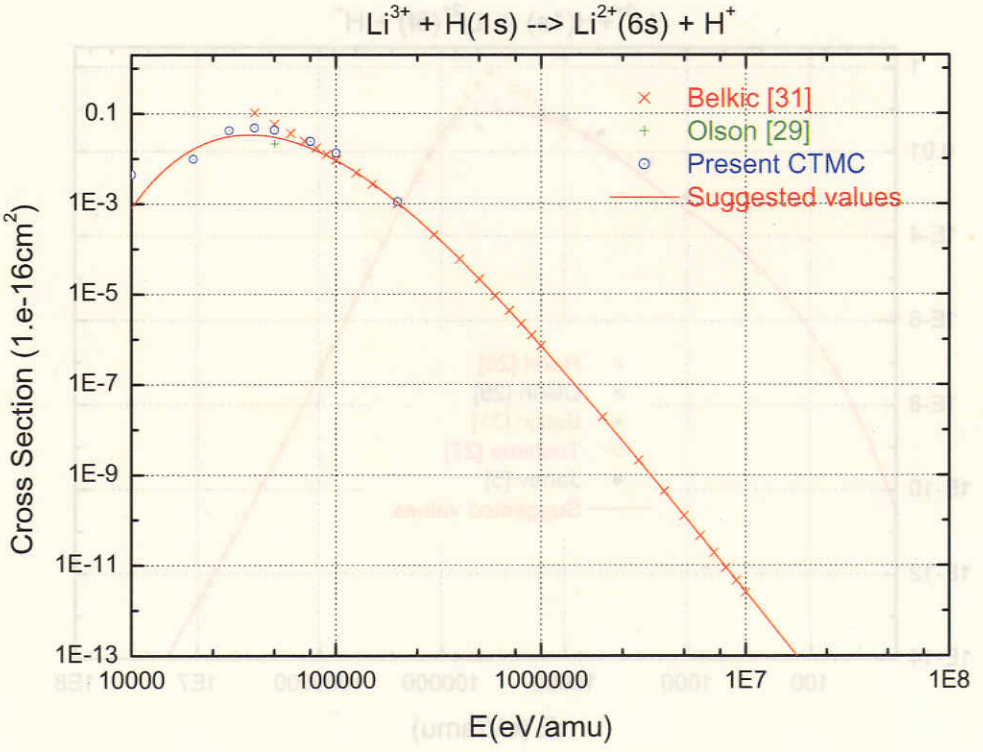

Figure 18. Same as in Fig.3, but for capture to $Li^{2+}(6s)$.

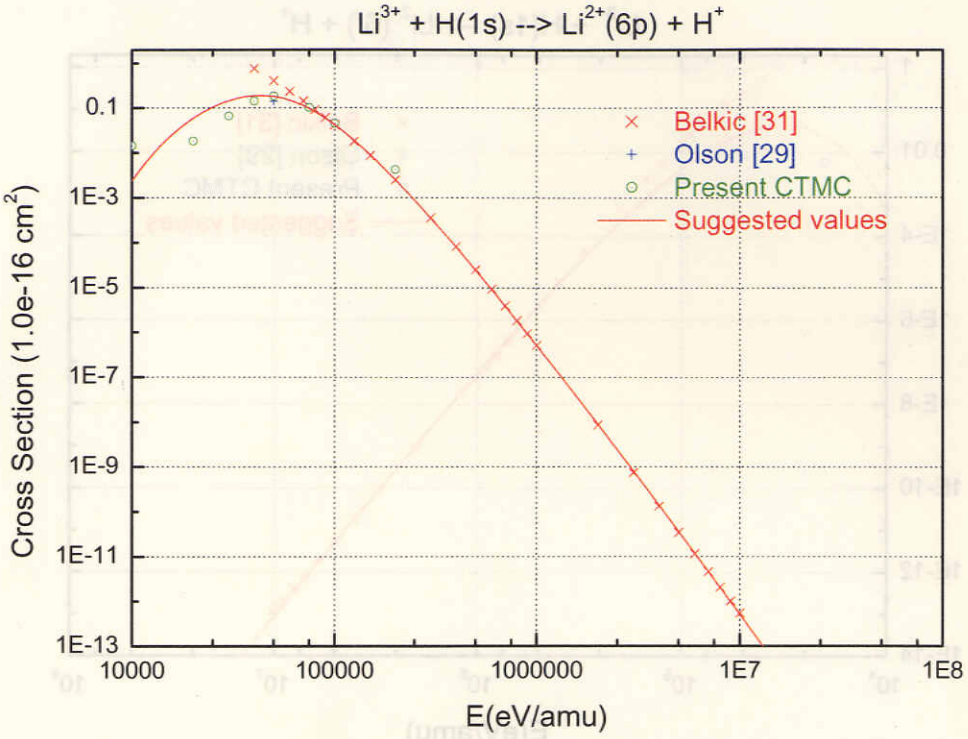

Figure 19. Same as in Fig.3, but for capture to $Li^{2+}(6p)$.

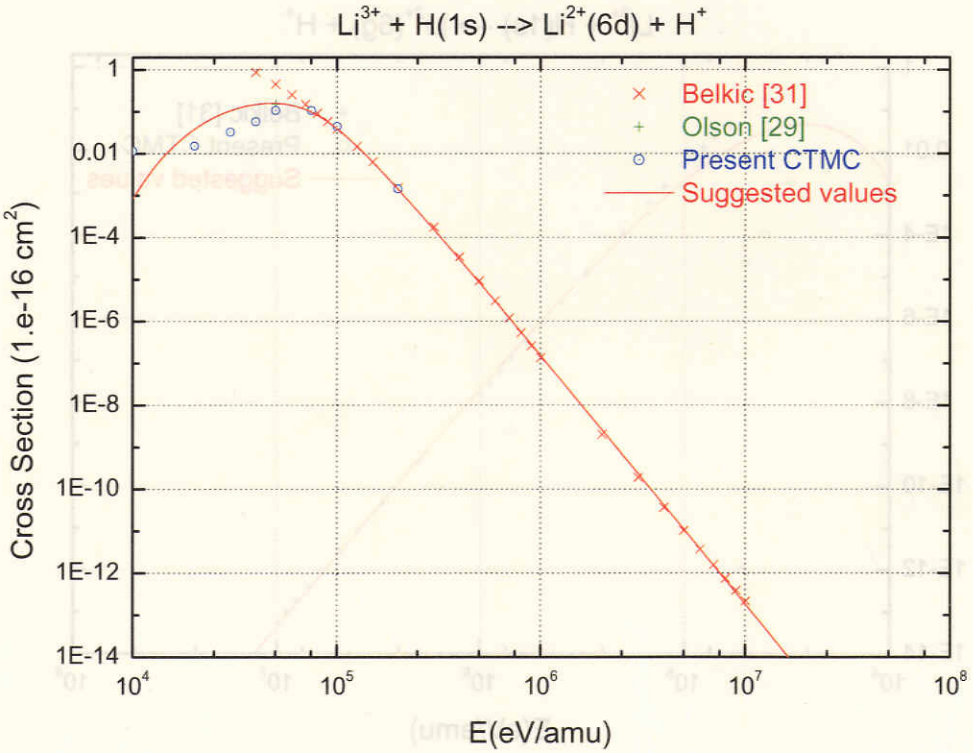

Figure 20. Same as in Fig.3, but for capture to $Li^{2+}(6d)$.

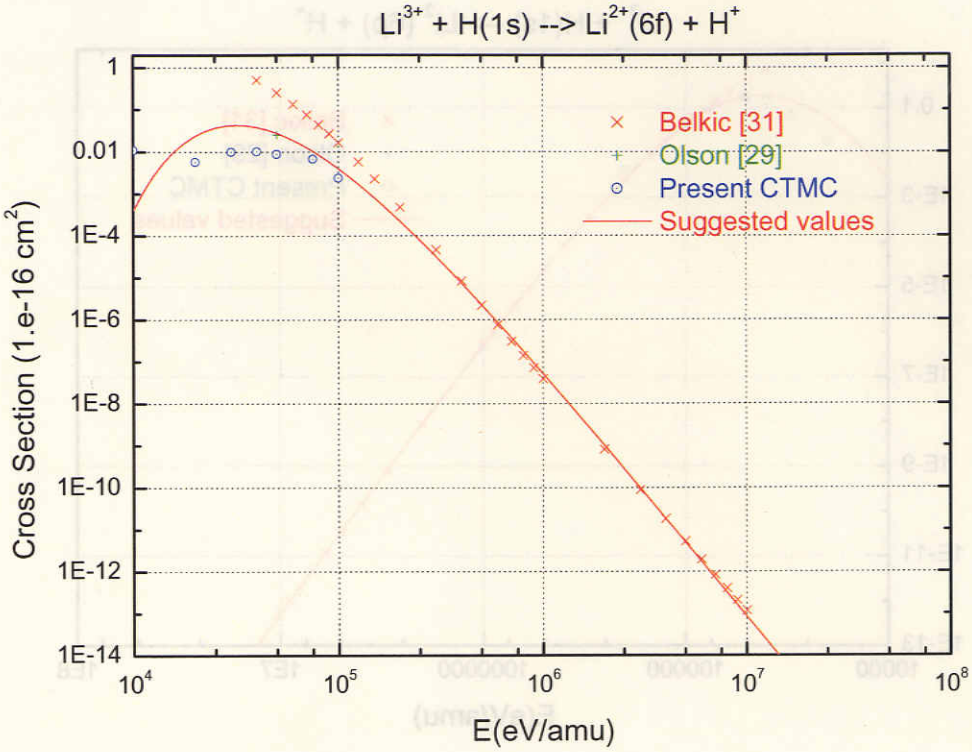

Figure 21. Same as in Fig.3, but for capture to $Li^{2+}(6f)$.

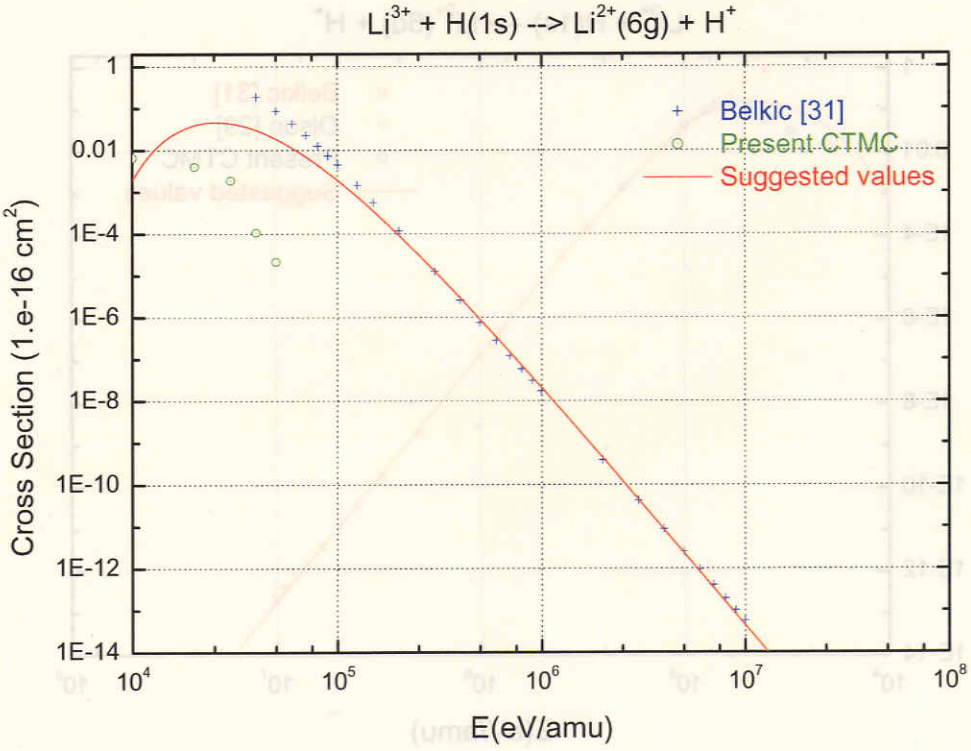

Figure 22. Same as in Fig.3, but for capture to $Li^{2+}(6g)$.

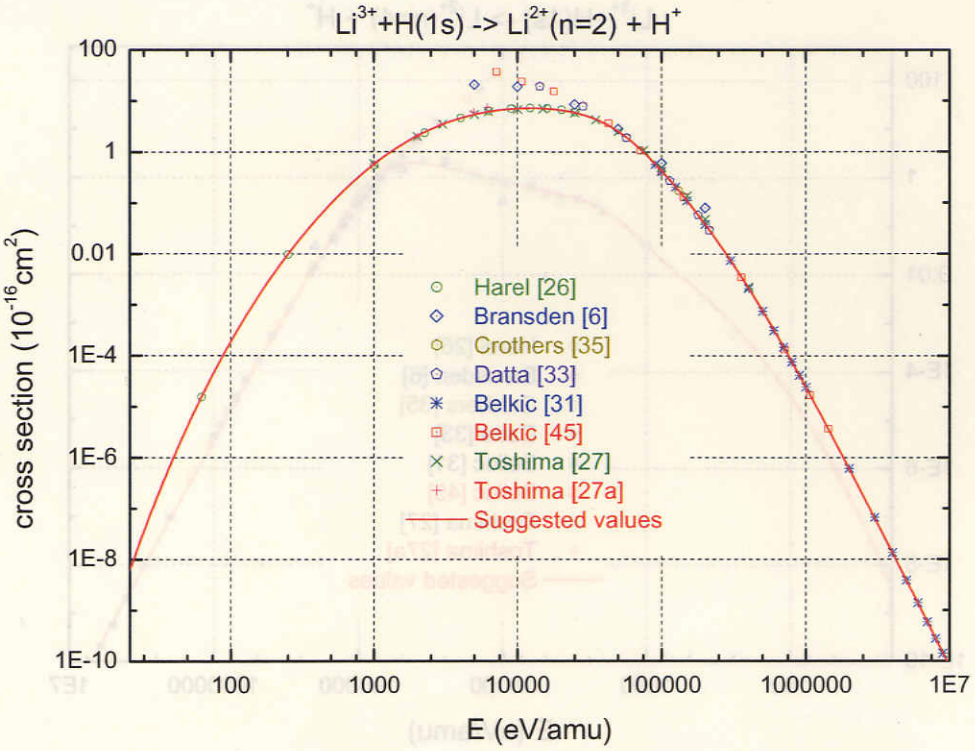

Figure 23. Fit (full line) of preferred electron capture cross section to $Li^{2+}(n=2)$ level in collisions of Li^{3+} with H(1s).

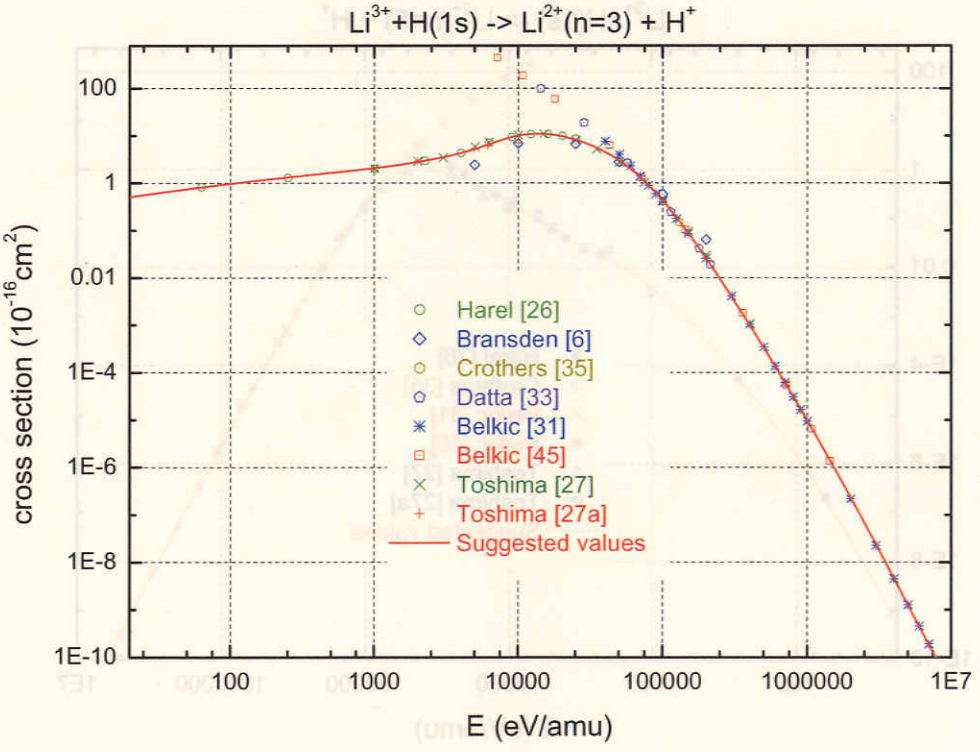

Figure 24. Same as in Fig.23, but for capture to $Li^{2+}(n=3)$.

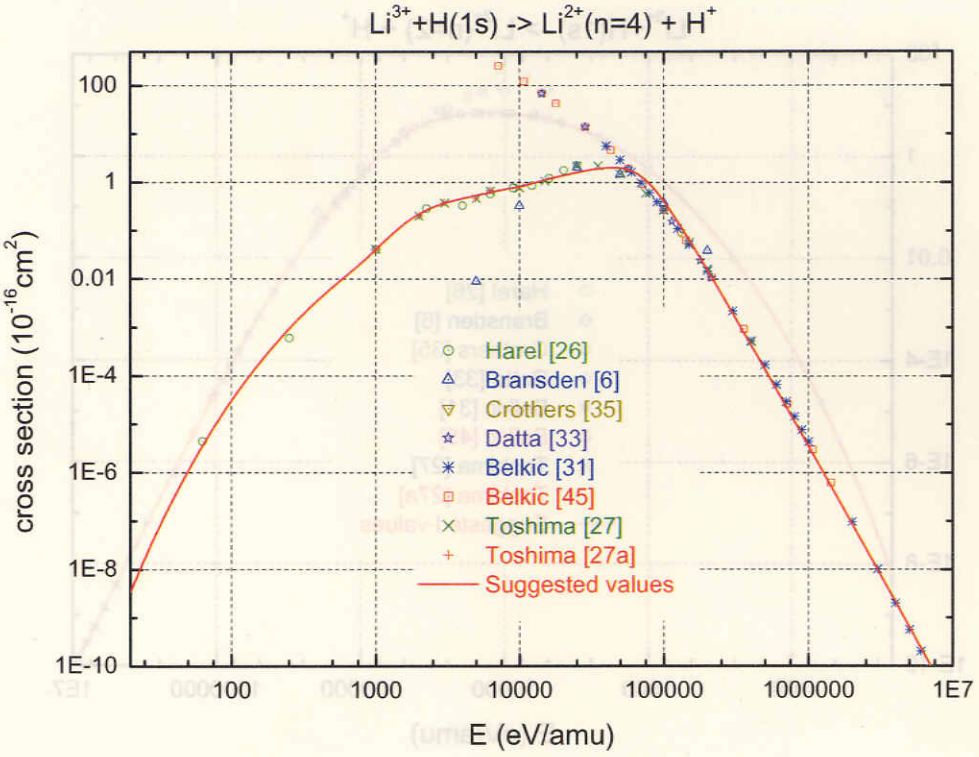

Figure 25. Same as in Fig.23, but for capture to $Li^{2+}(n=4)$.

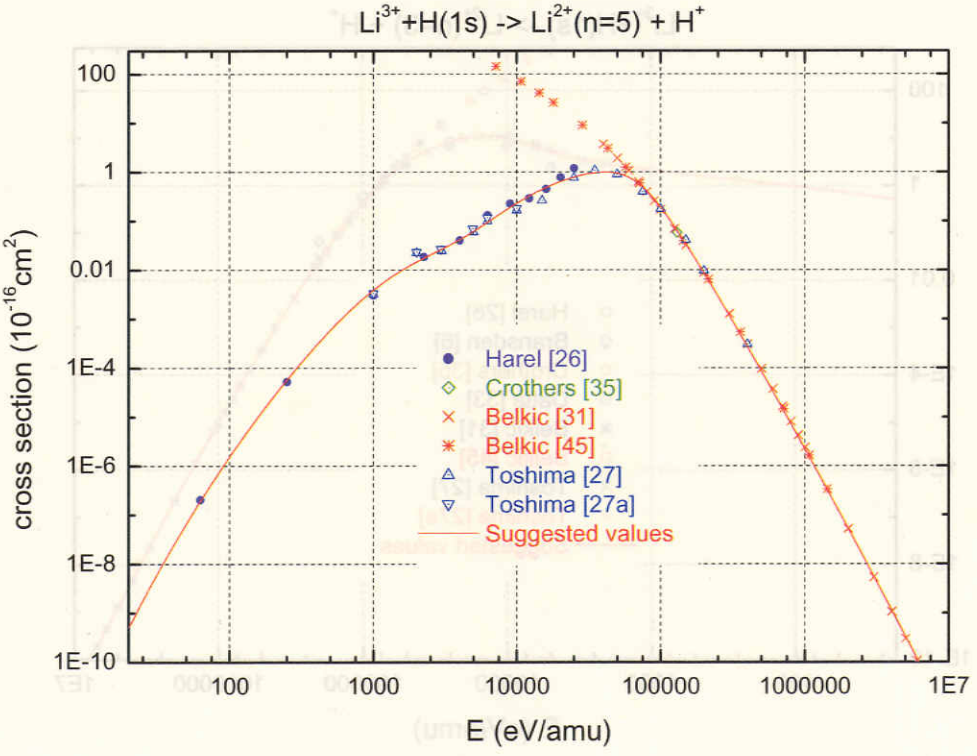

Figure 26. Same as in Fig.23, but for capture to $Li^{2+}(n=5)$.

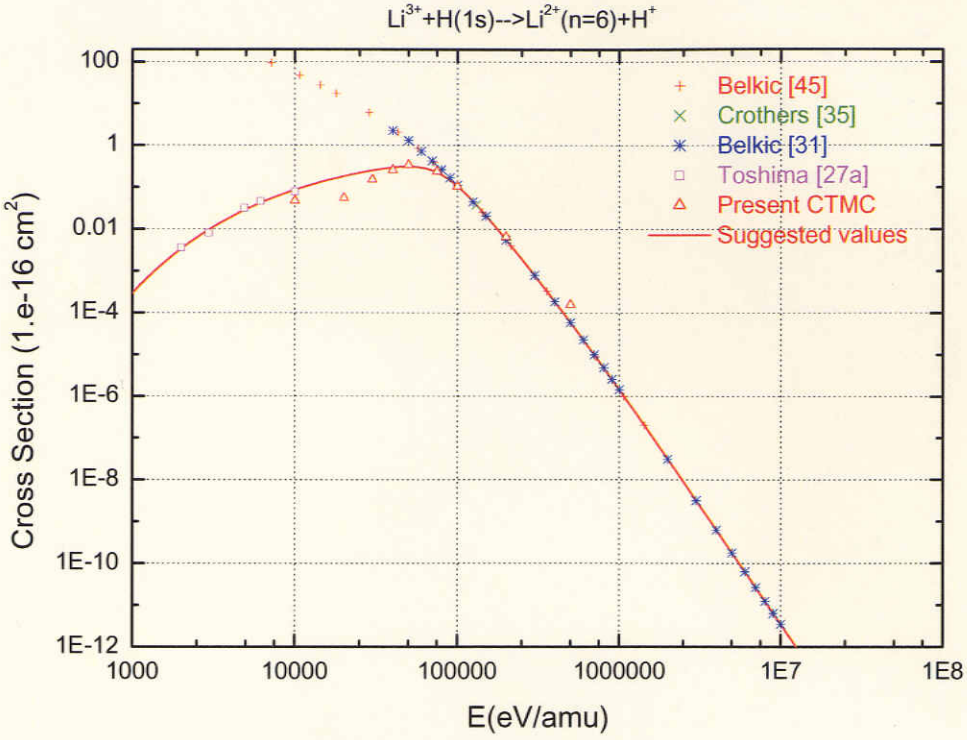

Figure 27. Same as in Fig.23, but for capture to $Li^{2+}(n=6)$.

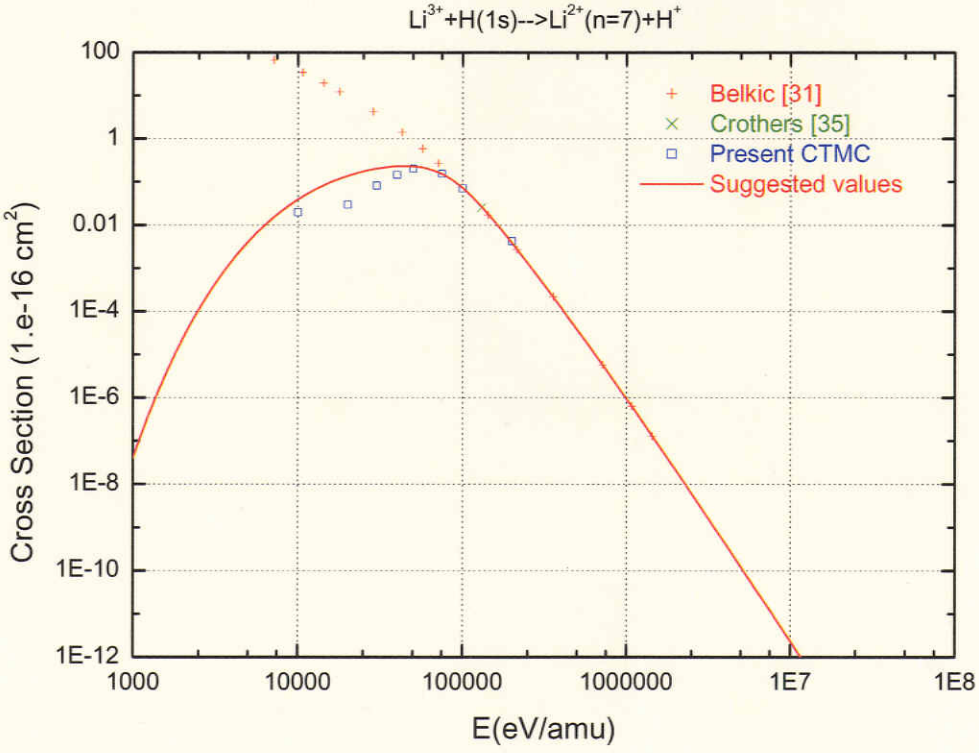

Figure 28. Same as in Fig.23, but for capture to $Li^{2+}(n=7)$.

Recent Issues of NIFS-DATA Series

NIFS-DATA-61 U.I. Safronova, C. Namba, I. Murakami, W.R. Johnson and M.S. Safronova,
E1,E2, M1, and M2 Transitions in the Neon Isoelectronic Sequence: Jan. 2001

NIFS-DATA-62 R. K. Janev, Yu.V. Ralchenko, T. Kenmotsu,
Unified Analytic Formula for Physical Sputtering Yield at Normal Ion Incidence: Apr. 2001

NIFS-DATA-63 Y. Itikawa,
Bibliography on Electron Collisions with Molecules: Rotational and Vibrational Excitations, 1980-2000 Apr. 2001

NIFS-DATA-64 R.K. Janev, J.G. Wang and T.Kato,
Cross Sections and Rate Coefficients for Charge Exchange Reactions of Protons with Hydrocarbon Molecules: May 2001

NIFS-DATA-65 T. Kenmotsu, Y. Yamamura, T. Ono and T. Kawamura,
A New Formula of the Energy Spectrum of Sputtered Atoms from a Target Material Bombarded with Light Ions at Normal Incidence: May 2001

NIFS-DATA-66 I. Murakami, U. I. Safronova and T. Kato,
Dielectronic Recombination Rate Coefficients to Excited States of Be-like Oxygen: May 2001

NIFS-DATA-67 N. Matsunami, E. Hatanaka, J. Kondoh, H. Hosaka, K. Tsumori, H. Sakaue and H. Tawara,
Secondary Charged Particle Emission from Proton Conductive Oxides by Ion Impact: July 2001

NIFS-DATA-68 R.K. Janev, J.G. Wang, I. Murakami and T. Kato,
Cross Sections and Rate Coefficients for Electron-Impact Ionization of Hydrocarbon Molecules: Oct. 2001

NIFS-DATA-69 S. Zou, T. Kato, I. Murakami,
Charge Exchange Recombination Spectroscopy of Li III Ions for Fusion Plasma Diagnostics: Oct. 2001

NIFS-DATA-70 I. Murakami, T. Kato, A. Igarashi, M. Imai, Y. Itikawa, D. Kato, M. Kimura, T. Kusakabe, K. Moribayashi, T. Morishita, K. Motohashi, L. Pichl AMDIS and CHART update (I): Oct. 2002

NIFS-DATA-71 S. Zou, L. Pichl, M. Kimura and T. Kato
Total, Partial and Differential Ionization Cross Sections in Proton-hydrogen Collisions at Low Energy: Jan. 2003

NIFS-DATA-72 M. Hayashi
Bibliography of Electron and Photon Cross Sections with Atoms and Molecules Published in the 20th Century – Argon –: Jan. 2003

NIFS-DATA-73 J. Horacek, K. Houfek, M. Cizek, I. Murakami and T. Kato
Rate Coefficients for Low-Energy Electron Dissociative Attachment to Molecular Hydrogen: Feb. 2003

NIFS-DATA-74 M. Hayashi
Bibliography of Electron and Photon Cross Sections with Atoms and Molecules Published in the 20th Century – Carbon Dioxide –: Apr. 2003

NIFS-DATA-75 X. Ma, H.P. Liu, Z.H. Yang, Y.D. Wang, X.M. Chen, Z.Y. Liu, I. Murakami and C. Namba
Cross-section Data Measured at Low Impact Energies for Ar^{q+} Ions on Argon and Neon Targets. Apr. 2003

NIFS-DATA-76 M. Hayashi
Bibliography of Electron and Photon Cross Sections with Atoms and Molecules Published in the 20th Century – Sulphur Hexafluoride –: May 2003

NIFS-DATA-77 M. Hayashi
Bibliography of Electron and Photon Cross Sections with Atoms and Molecules Published in the 20th Century – Nitrogen Molecule – : June 2003

NIFS-DATA-78 A. Iwamae, T. Fujimoto, H. Zhang, D. P. Kilcrease, G. Csanak and K.A. Berrington
Population Alignment Collisional Radiative Model for Helium-like Carbon:Polarization of Emission Lines and Anisotropy of the Electron Velocity Distribution Function in Plasmas: Aug. 2003

NIFS-DATA-79 M. Hayash
i Bibliography of Electron and Photon Cross Sections with Atoms and Molecules Published in the 20th Century – Xenon – ; Sep. 2003

NIFS-DATA-80 M. Hayashi
Bibliography of Electron and Photon Cross Sections with Atoms and Molecules Published in the 20th Century – Halogen Molecules – ; Dec. 2003

NIFS-DATA-81 M. Hayashi
Bibliography of Electron and Photon Cross Sections with Atoms and Molecules Published in the 20th Century – Water vapour – : Dec. 2003

NIFS-DATA-82 M. Hayashi
Bibliography of Electron and Photon Cross Sections with Atoms and Molecules Published in the 20th Century – Hydrogen molecules – : Feb. 2004

NIFS-DATA-83 M. Hayashi
Bibliography of Electron and Photon Cross Sections with Atoms and Molecules Published in the 20th Century – Hydrogen Halide Molecules – : Mar. 2004

NIFS-DATA-84 ELECTRAN - Monte Carlo Program of Secondary Electron Emission from Monoatomic Solids under the Impact of 0.1 - 10 keV Electrons: Mar. 2004

NIFS-DATA-85 I. Murakami, T. Kato, U.I. Safronova and A.A. Vasilyev,
Dielectronic Recombination Rate Coefficients to Excited States of Boronlike Oxygen and Dielectronic Satellite Lines: May 2004

NIFS-DATA-86 I. Murakami , J. Yan , H. Sato , M. Kimura , R. K. Janev , T. Kato,
Collision Processes of Li3+ with Atomic Hydrogen: Cross Section Database:Aug.2004